

Fermi-Surface Nesting in Reverse from Local-Moment Description of Iron-Pnictide High- T_c Superconductors

J P Rodriguez¹, M A N Araujo^{2,3}, P D Sacramento³

¹ Department of Physics and Astronomy, California State University at Los Angeles, Los Angeles, CA 90032

² Departamento de Física, Universidade de Évora, P-7000-671, Évora, Portugal

³ CFIF, Instituto Superior Técnico, TU Lisbon, Av. Rovisco Pais, 1049-001 Lisboa, Portugal

E-mail: jrodrig@calstatela.edu

Abstract. We uncover the low-energy spectrum of a two-orbital t - J model for electronic excitations in a square lattice of spin-1 iron atoms by employing Schwinger-boson-slave-fermion mean-field theory and by exact diagonalization of one hole that roams over a $4 \times 4 \times 2$ lattice. Holes propagate coherently within orbitals below a threshold Hund coupling when long-range antiferromagnetic order across the two orbitals is established by magnetic frustration that is off-diagonal in the orbital indices. This leads to two hole-pocket Fermi surfaces centered at zero two-dimensional (2D) momentum that are linked by the Goldstone mode associated with hidden magnetic order. Proximity to a commensurate spin-density wave (cSDW) metal that exists above the threshold Hund coupling results in additional electronic excitations on Fermi surface pockets centered at cSDW momenta, with 2D momentum that is carried primarily by low-energy spinwaves associated with cSDW order. We find that this inverse Fermi surface nesting mechanism is robust with respect to the addition of inter-orbital hopping.

PACS numbers: 74.70.Xa, 75.10.Jm, 75.30.Fv, 75.30.Ds, 71.10.Fd

Submitted to: *New J. Phys.*

1. Introduction

The surprising discovery of high-temperature superconductivity in iron-pnictide compounds is perhaps the newest unsolved puzzle in condensed matter physics[1]. Calculations of the electronic band structure that include all five iron $3d$ orbitals, but that assume only weak inter-electron repulsion, predict two-dimensional (2D) nested Fermi surface pockets centered at zero momentum and at wavenumbers $(\pi/a)\hat{x}$ and $(\pi/a)\hat{y}$ [2]. This prediction is consistent with determinations of the electronic structure in iron-pnictide systems by angle-resolved photoemission spectroscopy (ARPES) [3][4][5][6]. Here a denotes the lattice constant of the square lattice of iron atoms that stacks up to form iron-pnictide systems. Band structure calculations also predict an ordered magnetic moment of 2 Bohr magnetons (μ_B) in the commensurate spin-density wave (cSDW) state that exists in parent compounds at low temperature. The ordered cSDW moment that is measured in iron-pnictide systems by elastic neutron diffraction can be much smaller[7]. It reaches values as low as $0.3\mu_B$. Frustrated Heisenberg models that assume local magnetic moments at each iron atom can successfully account for the weak cSDW that exists in parent compounds[8][9][10][11], on the other hand. They can also give a good account of the low-energy spin excitations near cSDW momenta that have been uncovered in iron-pnictide systems by inelastic neutron scattering[12][13][14][15][16][17]. Such Heisenberg models have an insulating groundstate, however, that is a result of strong inter-electron repulsion. This fact conflicts with the metallic nature of iron-pnictide superconductors and their parent compounds.

Iron-pnictide high-temperature superconductors then appear to be simultaneously itinerant-electron metals and local-moment magnets. We identify a way to resolve this dilemma from the limit of strong inter-electron repulsion by injecting a low concentration of mobile charge carriers into a local-moment cSDW that experiences magnetic frustration that is off-diagonal in the orbital indices[9]. Both a Schwinger-boson-slave-fermion mean-field theory and exact computer calculations on a finite-size system find a quantum phase transition into a hidden half metal state as Hund's Rule coupling weakens[18]. The new groundstate shows long range antiferromagnetic order across the $d+ = 3d_{(x+iy)z}$ and $d- = 3d_{(x-iy)z}$ orbitals. We use the $d\pm$ orbitals because they are the least localized ones, and because they hence maximize Hund's Rule coupling. This orbital basis therefore maximizes the tendency to form local magnetic moments on each iron atom. The new hidden half metal state exhibits coherent intra-orbital hole motion, which yields two Fermi surface hole pockets centered at zero 2D momentum. Inter-orbital hopping fails to destroy the state. Instead, it can lead to an orbitally sensitive reverse Fermi-surface nesting mechanism near the quantum phase transition that is mediated by zero-energy cSDW spin-wave excitations. (See Figs. 9 and 12.) The latter, in particular, can result in a nested "electron" Fermi surface pocket at wavenumber $(\pi/a)\hat{x}(\hat{y})$ with predominantly $3d_{yz}(3d_{xz})$ orbital character. Mean-field theory predicts that the single-particle excitations here show a mixture of electron and

hole dispersion[18]. We now pass to the analysis of the theoretical model.

2. Two-Orbital t - J Model

We shall now introduce a two-orbital t - J model that describes the low-energy electronic excitations in iron-pnictide high-temperature superconductors[18]. Spin-1/2 moments exist over the $3d_{(x+iy)z}$ and $3d_{(x-iy)z}$ orbitals at each iron atom. These are the least localized orbitals within the 2D subspace spanned by the degenerate $3d_{xz}$ and $3d_{yz}$ orbitals, and they therefore result in the largest possible Hund's Rule coupling constant, $-J_0$. This fact is demonstrated explicitly in the Appendix for the case of hydrogenic $3d$ orbitals with the bare Coulomb interaction. In contrast, the commonly used $3d_{xz}$ and $3d_{yz}$ orbitals from Chemistry are the most localized ones within the same 2D subspace[19][20][21], and they result in the smallest possible Hund's Rule coupling. The isotropic nature of the $3d_{(x\pm iy)z}$ orbitals also implies isotropic Heisenberg exchange coupling constants J_1 and J_2 across nearest-neighbor and next-nearest-neighbor links of the square lattice of iron atoms within each iron-pnictide layer. The two-orbital t - J model over a square-lattice of iron atoms in an isolated layer then reads

$$H = - \sum_{\langle i,j \rangle} \sum_{\alpha,\beta} \sum_s (t_1^{\alpha,\beta} \tilde{c}_{i,\alpha,s}^\dagger \tilde{c}_{j,\beta,s} + \text{h.c.}) - \sum_{\langle\langle i,j \rangle\rangle} \sum_{\alpha,\beta} \sum_s (t_2^{\alpha,\beta} \tilde{c}_{i,\alpha,s}^\dagger \tilde{c}_{j,\beta,s} + \text{h.c.}) \\ + \frac{1}{2} J_0 \sum_i \left[\sum_\alpha \mathbf{S}_{i,\alpha} \right]^2 + \sum_{\langle i,j \rangle} \sum_{\alpha,\beta} J_1^{\alpha,\beta} \mathbf{S}_{i,\alpha} \cdot \mathbf{S}_{j,\beta} + \sum_{\langle\langle i,j \rangle\rangle} \sum_{\alpha,\beta} J_2^{\alpha,\beta} \mathbf{S}_{i,\alpha} \cdot \mathbf{S}_{j,\beta}. \quad (1)$$

Above, $\mathbf{S}_{i,\alpha}$ is the spin operator that acts on the spin $s_0 = 1/2$ state localized on orbital α at site i , while $\tilde{c}_{i,\alpha,s}^\dagger$ is the corresponding electron creation operator that takes into account the constraint against double-occupancy at a site-orbital. The orbitals α are either $d+ = 3d_{(x+iy)z}$ or $d- = 3d_{(x-iy)z}$, while the sites i run over the square lattice of iron atoms. The isotropy and the degeneracy of this pair of orbital states yields two independent and isotropic Heisenberg exchange coupling constants for nearest-neighbor and for next-nearest-neighbor links, $\langle i, j \rangle$ and $\langle\langle i, j \rangle\rangle$, respectively, $n = 1$ and 2 :

$$J_n^{d+,d+} = J_n^\parallel = J_n^{d-,d-} \quad \text{and} \quad J_n^{d+,d-} = J_n^\perp = J_n^{d-,d+}. \quad (2)$$

Correlated hopping of an electron in orbital β to a neighboring unoccupied orbital α is controlled by the hopping matrix elements $t_1^{\alpha,\beta}$ and $t_2^{\alpha,\beta}$. Let us take real hopping matrix elements in the $(3d_{xz}, 3d_{yz})$ orbital basis[22]. The hopping matrix elements in the present $d\pm$ basis are then given by

$$t_n^{d\pm,d\pm} = \frac{1}{2} [t_n^{x,x} + t_n^{y,y}] \pm \frac{i}{2} [t_n^{x,y} - t_n^{y,x}], \quad (3a)$$

$$t_n^{d\pm,d\mp} = \frac{1}{2} [t_n^{x,x} - t_n^{y,y}] \mp \frac{i}{2} [t_n^{x,y} + t_n^{y,x}]. \quad (3b)$$

The symmetry relation $t_{1(2)}^{x,y} = t_{1(2)}^{y,x}$ in the $(3d_{xz}, 3d_{yz})$ orbital basis then yields diagonal hopping matrix elements that are real and isotropic in the $(d+, d-)$ basis:

$$t_1^{d\pm,d\pm}(\hat{\mathbf{x}}) = t_1^{d\pm,d\pm}(\hat{\mathbf{y}}) \quad \text{and} \quad \text{Im } t_1^{d\pm,d\pm} = 0, \quad (4a)$$

$$t_2^{d\pm, d\pm}(\hat{\mathbf{x}} + \hat{\mathbf{y}}) = t_2^{d\pm, d\pm}(\hat{\mathbf{y}} - \hat{\mathbf{x}}) \quad \text{and} \quad \text{Im } t_2^{d\pm, d\pm} = 0. \quad (4b)$$

The off-diagonal hopping matrix elements $t_n^{d\pm, d\mp}$ have d -wave symmetry, on the other hand. Also, the identities $t_1^{x,y} = 0 = t_1^{y,x}$ yields real off-diagonal hopping matrix elements across nearest neighbors, while the symmetry relation $t_2^{x,x} = t_2^{y,y}$ yields pure-imaginary off-diagonal hopping matrix elements across next-nearest neighbors:

$$t_1^{d\pm, d\mp}(\hat{\mathbf{x}}) = -t_1^{d\pm, d\mp}(\hat{\mathbf{y}}) \quad \text{and} \quad \text{Im } t_1^{d\pm, d\mp} = 0, \quad (5a)$$

$$t_2^{d\pm, d\mp}(\hat{\mathbf{x}} + \hat{\mathbf{y}}) = -t_2^{d\pm, d\mp}(\hat{\mathbf{y}} - \hat{\mathbf{x}}) \quad \text{and} \quad \text{Re } t_2^{d\pm, d\mp} = 0. \quad (5b)$$

Henceforth, we shall change the notation for the hopping matrix elements to $t_{1(2)}^{\parallel} = t_{1(2)}^{d\pm, d\pm}$, to $t_1^{\perp} = t_1^{d\pm, d\mp}$, and to $-t_2^{d-, d+} = t_2^{\perp} = t_2^{d+, d-}$.

Last, it is useful to point out that because t_1^{\perp} is real, a global swap of the orbitals, $d\pm \rightarrow d\mp$, is an exact symmetry of the two-orbital t - J model (1) in the absence of next-nearest neighbor inter-orbital hopping: $t_2^{\perp} = 0$. Let $P_{d\bar{d}}$ denote the global swap operation of the $d+$ and $d-$ orbitals. Eigenstates of the t - J model Hamiltonian (1) are then even (+) or odd (-) under it, with respective forms $|\Psi\rangle \pm P_{d\bar{d}}|\Psi\rangle$. Further, in the limit $J_0 \rightarrow -\infty$ where Hund's Rule is obeyed, a spin triplet state exists at iron atoms that do not have any holes. Such spin-1 local moments are clearly even under $P_{d\bar{d}}$. This implies that a one-hole state that is even under $P_{d\bar{d}}$ has a local $3d_{xz}$ orbital when Hund's Rule is obeyed, and that a one-hole state that is odd under $P_{d\bar{d}}$ has a local $3d_{yz}$ orbital! At the opposite extreme $J_0 \rightarrow +\infty$ where Hund's Rule is maximally violated, a spin singlet state exists at iron atoms without any holes. Such spin-0 iron sites are clearly odd under $P_{d\bar{d}}$. In the case of an even number of iron sites, this implies that a one-hole state that is even under $P_{d\bar{d}}$ instead has a local $3d_{yz}$ orbital, and that a one-hole state that is odd under $P_{d\bar{d}}$ instead has a local $3d_{xz}$ orbital! One-hole states that are even or odd under $P_{d\bar{d}}$ must then have a mixture of $3d_{xz}$ and $3d_{yz}$ orbital character at finite Hund's Rule coupling by continuity.

And because t_2^{\perp} is pure imaginary, the global orbital swap operation is an exact symmetry in the absence of nearest neighbor inter-orbital hopping, $t_1^{\perp} = 0$, after making the global gauge transformation of the orbitals $|d\pm\rangle \rightarrow i^{\pm 1/2}|d\pm\rangle$. Eigenstates of the t - J model Hamiltonian (1) are then even (+) or odd (-) under the combined operation $P'_{d\bar{d}}$, where they have the form $|\Psi\rangle \pm P'_{d\bar{d}}|\Psi\rangle$. Notice that the global gauge transformation rotates the orbital axes by 45 degrees. Repeating the previous arguments yields that a one-hole state that is even under $P'_{d\bar{d}}$ has a local $3d_{x'z}$ orbital when Hund's Rule is obeyed, and that a one-hole state that is odd under $P'_{d\bar{d}}$ has a local $3d_{y'z}$ orbital in such case. Here (x', y') denote the planar orbital coordinates along the next-nearest neighbor links.

3. Hidden Half Metal State

In general, the Heisenberg exchange constants have a direct ferromagnetic contribution from the exchange Coulomb integral (see Appendix) and an indirect antiferromagnetic

contribution from the super-exchange mechanism through the pnictide atom[23]:

$$J_{1(2)}^{\alpha,\beta} = J_{1(2)}^{\alpha,\beta}(\text{drct}) + J_{1(2)}^{\alpha,\beta}(\text{sprx}). \quad (6)$$

We shall assume that the super-exchange contribution is independent of the orbital indices: $J_{1(2)}^{\alpha,\beta}(\text{sprx}) = J_{1(2)}^{(\text{sprx})}$. This is the case if the pnictide orbital in question is the p_x , p_y , or p_z one, for example. Recent density-functional calculations for the electronic structure of iron-pnictide materials find that direct exchange and super exchange can cancel out across nearest neighbors[24][25]. We shall assume that this is the case for nearest-neighbor Heisenberg exchange across the same orbital: $J_1^{\parallel} = 0$. It is further reasonable to assume that $J_{1(2)}^{d\pm,d\mp}(\text{drct})$ is smaller in magnitude than $J_{1(2)}^{d\pm,d\pm}(\text{drct})$. This assumption is borne out in the limit of large overlap between neighboring iron 3d orbitals (see Appendix), where $-J_{1(2)}^{d\pm,d\mp}(\text{drct})$ is 10 times smaller than $-J_{1(2)}^{d\pm,d\pm}(\text{drct})$! We are then left with a net antiferromagnetic Heisenberg exchange across nearest neighbors between different orbitals due to super-exchange: $J_1^{\perp} > 0$. Last, the previous DFT calculations find that $J_2^{\alpha,\beta}(\text{drct})$ is negligible. This leaves antiferromagnetic Heisenberg exchange across next-nearest neighbors due to super-exchange, which we assume is invariant with respect to a rotation of the orbital basis: $J_2^{\parallel} = J_2^{\perp} > 0$.

In the absence of mobile holes, the off-diagonal magnetic frustration described by the above list of Heisenberg exchange constants results in a commensurate spin-density wave (cSDW) along one of the principal axes of the square lattice of iron atoms at strong Hund's Rule coupling, $-J_0$, and for $J_2 > J_1/2$. Here $J_{1(2)} = (J_{1(2)}^{\parallel} + J_{1(2)}^{\perp})/2$. An antiferromagnetic state with opposing ferromagnetic order over the $d+$ and the $d-$ orbitals appears at Hund's Rule coupling below a critical value of $-J_{0c} = 2(J_1^{\perp} - J_1^{\parallel}) - 4J_2^{\parallel}$ in the large- s_0 limit[11]. The latter marks a quantum-critical phase transition between the cSDW at strong Hund's Rule coupling and the hidden ferromagnet at weak Hund's Rule coupling. (Cf. Fig. 1.) Observe now that injecting mobile holes while inter-orbital hopping is suppressed preserves the $\nearrow_{d+} \searrow_{d-}$ spin order of the hidden ferromagnetic state in the classical limit[11]. This is a semi-classical picture of a hidden half metal state with coherent intra-orbital propagation of holes that follows the dispersion relation

$$\varepsilon_e(\mathbf{k}) = -2t_1^{\parallel}(\cos k_x a + \cos k_y a) - 2t_2^{\parallel}(\cos k_+ a + \cos k_- a), \quad (7)$$

where $k_{\pm} = k_x \pm k_y$. It implies two degenerate hole Fermi surface pockets centered at zero momentum when $t_1^{\parallel} < 0$ and $t_1^{\parallel} + 2t_2^{\parallel} < 0$, in qualitative agreement with ARPES on iron-pnictide superconductors. Below, we shall demonstrate that the hidden half-metal state is robust with respect to the addition of inter-orbital hopping. We will also show that a reverse SDW nesting effect exists at the quantum-critical point that separates the hidden half-metal state from the cSDW state. It results in copies of the hole Fermi-surface pockets centered at cSDW wavenumbers $(\pi/a)\hat{\mathbf{x}}$ and $(\pi/a)\hat{\mathbf{y}}$. We shall see that the latter have mixed electron and hole character according to meanfield theory.

3.1. Schwinger-Boson-Slave-Fermion Mean-field Theory

Unlike the doped Néel state in the one-orbital nearest-neighbor t - J model for copper-oxygen planes in high- T_c superconductors[26][27], hole propagation in the hidden half

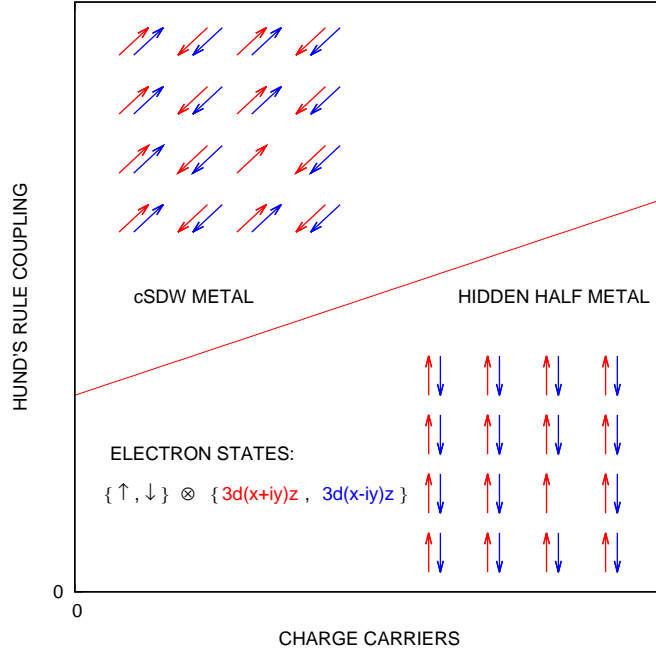


Figure 1. Shown is the phase diagram obtained from the Schwinger-boson-slave-fermion mean-field theory of the two-orbital t - J model, Eq. (1). The red line marks a quantum-critical point that separates a charge-carrier poor cSDW metal from a charge-carrier rich hidden half metal at fixed Hund's Rule coupling.

metal does not produce strings of overturned spins that disrupt the antiferromagnetic $\nwarrow_{d+} \searrow_{d-}$ order when inter-orbital hopping is absent. This suggests that the mean-field approximation for the Schwinger-boson-slave-fermion formulation of the two-orbital t - J model (1) is applicable for this state at weak inter-orbital hopping. The constraint against double occupancy is enforced by expressing the correlated electron annihilation operator as $\tilde{c}_{i,\alpha,s} = b_{i,\alpha,s} f_{i,\alpha}^\dagger$ along with the new constraint

$$2s_0 = b_{i,\alpha,\uparrow}^\dagger b_{i,\alpha,\uparrow} + b_{i,\alpha,\downarrow}^\dagger b_{i,\alpha,\downarrow} + f_{i,\alpha}^\dagger f_{i,\alpha} \quad (8)$$

per site i , per orbital α , where $s_0 = 1/2$ is the electron spin [28][29]. Here, $b_{i,\alpha,\uparrow}$ and $b_{i,\alpha,\downarrow}$ are the annihilation operators for the pair of Schwinger bosons, while $f_{i,\alpha}$ is the annihilation operator for the spinless slave fermion. The spin operator is then expressed in the usual way: $\mathbf{S}_{i,\alpha} = \frac{1}{2}\hbar \sum_{s,s'} f_{i,\alpha} b_{i,\alpha,s}^\dagger \boldsymbol{\sigma}_{s,s'} b_{i,\alpha,s'} f_{i,\alpha}^\dagger$. Henceforth, we shall average the dynamics of the slave fermions over the bulk by writing $\mathbf{S}_{i,\alpha} \cong (1-x)\frac{1}{2}\hbar \sum_{s,s'} b_{i,\alpha,s}^\dagger \boldsymbol{\sigma}_{s,s'} b_{i,\alpha,s'}$ instead. Here, x denotes the concentration of holes per orbital. Following Arovas and Auerbach[30][31], we introduce symmetric versus antisymmetric meanfields with respect to spin flip for the ferromagnetic versus the antiferromagnetic links of the hidden ferromagnetic state (Fig. 1):

$$\langle b_{i,d\pm,\downarrow}^\dagger b_{j,d\pm,\downarrow} \rangle = Q_n^\parallel = \langle b_{i,d\pm,\uparrow}^\dagger b_{j,d\pm,\uparrow} \rangle \quad (n = 1, 2), \quad (9)$$

$$\pm \langle b_{i,d\pm,\downarrow}^\dagger b_{j,d\mp,\uparrow} \rangle = Q_n^\perp = \mp \langle b_{i,d\pm,\uparrow}^\dagger b_{j,d\mp,\downarrow} \rangle \quad (n = 0, 1, 2), \quad (10)$$

where $j = i$ for on-site links $n = 0$, where $j = i + \hat{x}(\hat{y})$ for nearest-neighbor links $n = 1$, and where $j = i \pm \hat{x} + \hat{y}$ for next-nearest-neighbor links $n = 2$. Next, we introduce

meanfields associated with hopping by slave fermions:

$$\frac{1}{2}\langle f_{i,d+}^\dagger f_{j,d+} \rangle = P_n^\parallel = \frac{1}{2}\langle f_{i,d-}^\dagger f_{j,d-} \rangle, \quad (11)$$

$$\frac{1}{2}\langle f_{i,d+}^\dagger f_{j,d-} \rangle^* = P_n^\perp = \frac{1}{2}\langle f_{i,d-}^\dagger f_{j,d+} \rangle \quad (n = 1, 2). \quad (12)$$

Last, we introduce meanfields associated with hopping of the Schwinger bosons across different orbitals:

$$\langle b_{i,d+,s}^\dagger b_{j,d-,s} \rangle^* = R_n^\perp = \langle b_{i,d-,s}^\dagger b_{j,d+,s} \rangle \quad (n = 1, 2), \quad (13)$$

where $s = \uparrow, \downarrow$. Now assume that all of the mean fields are homogeneous, and assume that the mean fields $P_{1(2)}^\parallel$, $Q_{1(2)}^\parallel$ and $Q_{1(2)}^\perp$ are isotropic. The mean-field approximation for the t - J model Hamiltonian (1) then has the form $H_{MF} = H_0[P, Q, R] + H_b^{(+)} + H_b^{(-)} + H_f$, where

$$\begin{aligned} H_0 = & 2 \sum_i J'_0 Q_0^\perp Q_0^{\perp*} + \\ & 2 \sum_{\langle i,j \rangle} \sum_\alpha [-(2t_1^\parallel Q_1^\parallel P_1^\parallel + \text{c.c.}) - (2t_1^\perp R_1^\perp P_1^\perp + \text{c.c.}) - J_1'^\parallel Q_1^\parallel Q_1^{\parallel*} + J_1'^\perp Q_1^\perp Q_1^{\perp*}] + \\ & 2 \sum_{\langle\langle i,j \rangle\rangle} \sum_\alpha [-(2t_2^\parallel Q_2^\parallel P_2^\parallel + \text{c.c.}) - (2t_2^\perp R_2^\perp P_2^\perp + \text{c.c.}) - J_2'^\parallel Q_2^\parallel Q_2^{\parallel*} + J_2'^\perp Q_2^\perp Q_2^{\perp*}] \end{aligned}$$

consolidates the bilinear terms among the mean fields, where

$$H_b^{(+)} = \frac{1}{2} \sum_{\mathbf{k}} \begin{bmatrix} b_{d+, \uparrow} \\ b_{d-, \uparrow} \\ \bar{b}_{d+, \downarrow}^\dagger \\ \bar{b}_{d-, \downarrow}^\dagger \end{bmatrix}^\dagger \begin{bmatrix} \Omega_\parallel & \Omega_\perp^* & 0 & +\Omega_\perp \\ \Omega_\perp' & \Omega_\parallel & -\Omega_\perp & 0 \\ 0 & -\Omega_\perp & \Omega_\parallel & \Omega_\perp' \\ +\Omega_\perp & 0 & \Omega_\perp^* & \Omega_\parallel \end{bmatrix} \begin{bmatrix} b_{d+, \uparrow} \\ b_{d-, \uparrow} \\ \bar{b}_{d+, \downarrow}^\dagger \\ \bar{b}_{d-, \downarrow}^\dagger \end{bmatrix}$$

and

$$H_b^{(-)} = \frac{1}{2} \sum_{\mathbf{k}} \begin{bmatrix} b_{d+, \downarrow} \\ b_{d-, \downarrow} \\ \bar{b}_{d+, \uparrow}^\dagger \\ \bar{b}_{d-, \uparrow}^\dagger \end{bmatrix}^\dagger \begin{bmatrix} \Omega_\parallel & \Omega_\perp^* & 0 & -\Omega_\perp \\ \Omega_\perp' & \Omega_\parallel & +\Omega_\perp & 0 \\ 0 & +\Omega_\perp & \Omega_\parallel & \Omega_\perp' \\ -\Omega_\perp & 0 & \Omega_\perp^* & \Omega_\parallel \end{bmatrix} \begin{bmatrix} b_{d+, \downarrow} \\ b_{d-, \downarrow} \\ \bar{b}_{d+, \uparrow}^\dagger \\ \bar{b}_{d-, \uparrow}^\dagger \end{bmatrix}$$

are the pair of Hamiltonians for free Schwinger bosons, with matrix elements

$$\Omega_\parallel(\mathbf{k}) = \lambda + 4 \sum_{n=1,2} (J_n'^\parallel Q_n^\parallel + 2t_n^\parallel P_n^\parallel) \gamma_n(\mathbf{k}), \quad (14)$$

$$\Omega_\perp(\mathbf{k}) = \sum_{n=0,1,2} z_n J_n'^\perp Q_n^\perp \gamma_n(\mathbf{k}), \quad (15)$$

$$\begin{aligned} \Omega_\perp'(\mathbf{k}) = & 4 \sum_{n=x,y} t_1^\perp(\hat{\mathbf{n}}) P_1^\perp(\hat{\mathbf{n}}) \cos(k_n a) \\ & + 4 \sum_{\pm} t_2^\perp(\hat{\mathbf{y}} \pm \hat{\mathbf{x}}) P_2^{\perp*}(\hat{\mathbf{y}} \pm \hat{\mathbf{x}}) \cos(k_\pm a), \end{aligned} \quad (16)$$

and where

$$H_f = \sum_{\mathbf{k}} \begin{bmatrix} f_{d+} \\ f_{d-} \end{bmatrix}^\dagger \begin{bmatrix} \varepsilon_\parallel & \varepsilon_\perp \\ \varepsilon_\perp^* & \varepsilon_\parallel \end{bmatrix} \begin{bmatrix} f_{d+} \\ f_{d-} \end{bmatrix}$$

is the Hamiltonian for free slave fermions, with matrix elements

$$\varepsilon_{\parallel}(\mathbf{k}) = 8 \sum_{n=1,2} t_n^{\parallel} Q_n^{\parallel} \gamma_n(\mathbf{k}), \quad (17)$$

$$\begin{aligned} \varepsilon_{\perp}(\mathbf{k}) = & 4 \sum_{n=x,y} t_1^{\perp}(\hat{\mathbf{n}}) R_1^{\perp}(\hat{\mathbf{n}}) \cos(k_n a) \\ & + 4 \sum_{\pm} t_2^{\perp}(\hat{\mathbf{y}} \pm \hat{\mathbf{x}}) R_2^{\perp}(\hat{\mathbf{y}} \pm \hat{\mathbf{x}}) \cos(k_{\pm} a). \end{aligned} \quad (18)$$

Above, the destruction operators for Schwinger bosons of momentum $\pm \mathbf{k}$ are defined by $b_{\alpha,s}(\mathbf{k}) = N_{\text{Fe}}^{-1/2} \sum_i e^{i\mathbf{k} \cdot \mathbf{r}_i} b_{i,\alpha,s}$ and $\bar{b}_{\alpha,s}(\mathbf{k}) = b_{\alpha,s}(-\mathbf{k})$, while the destruction operator for a slave fermion of momentum \mathbf{k} is $f_{\alpha}(\mathbf{k}) = N_{\text{Fe}}^{-1/2} \sum_i e^{i\mathbf{k} \cdot \mathbf{r}_i} f_{i,\alpha}$. Also above, $z_0 = 1$ and $z_{1(2)} = 4$ give the coordination number, and we define $\gamma_0(\mathbf{k}) = 1$, $\gamma_1(\mathbf{k}) = \frac{1}{2}(\cos k_x a + \cos k_y a)$, and $\gamma_2(\mathbf{k}) = \frac{1}{2}(\cos k_+ a + \cos k_- a)$, where $k_{\pm} = k_x \pm k_y$. Last, λ is the boson chemical potential that enforces the constraint against double occupancy (8) on *average* over the bulk of the system, and the effect of mobile holes on the Heisenberg spin-exchange is accounted for by the effective exchange coupling constants[29] $J' = (1 - x)^2 J$.

The spin-excitation spectrum of the hidden half metal state is obtained from the sum of the Schwinger bosons Hamiltonians, $H_b^{(+)} + H_b^{(-)}$, in two steps. We first make a two-orbital *Bogoliubov* transformation of the boson field:

$$b_{\alpha,s} = (\cosh \theta) \beta_{\alpha,s} - (\text{sgn } \alpha)(\text{sgn } s)(\sinh \theta) \bar{\beta}_{\alpha,\bar{s}}^{\dagger}, \quad (19a)$$

$$\bar{b}_{\alpha,\bar{s}}^{\dagger} = (\cosh \theta) \bar{\beta}_{\alpha,\bar{s}}^{\dagger} - (\text{sgn } \alpha)(\text{sgn } s)(\sinh \theta) \beta_{\alpha,s}, \quad (19b)$$

with $\cosh 2\theta = \Omega_{\parallel}/\omega_b^{(0)}$ and $\sinh 2\theta = \Omega_{\perp}/\omega_b^{(0)}$, where $\omega_b^{(0)} = (\Omega_{\parallel}^2 - \Omega_{\perp}^2)^{1/2}$. Here, we use the notation $\bar{d}\pm = d\mp$ in the orbital index and $\bar{s} = -s$ in the spin index. The sum $H_b^{(+)} + H_b^{(-)}$ then transforms to

$$\begin{aligned} H_b = & \frac{1}{2} \sum_{\mathbf{k}} \sum_{s=\uparrow,\downarrow} \begin{bmatrix} \beta_{d+,s} \\ \beta_{d-,s} \end{bmatrix}^{\dagger} \begin{bmatrix} \omega_b^{(0)} & \Omega'_{\perp} \\ \Omega'_{\perp} & \omega_b^{(0)} \end{bmatrix} \begin{bmatrix} \beta_{d+,s} \\ \beta_{d-,s} \end{bmatrix} \\ & + \frac{1}{2} \sum_{\mathbf{k}} \sum_{s=\uparrow,\downarrow} \begin{bmatrix} \bar{\beta}_{d+,s} \\ \bar{\beta}_{d-,s} \end{bmatrix}^{\text{T}} \begin{bmatrix} \omega_b^{(0)} & \Omega'_{\perp} \\ \Omega'_{\perp} & \omega_b^{(0)} \end{bmatrix} \begin{bmatrix} \bar{\beta}_{d+,s}^{\dagger} \\ \bar{\beta}_{d-,s}^{\dagger} \end{bmatrix}. \end{aligned}$$

Let $e^{2i\delta_b(\mathbf{k})}$ denote the phase factor of the inter-orbital matrix element $\Omega'_{\perp}(\mathbf{k})$, and let $k_0 = 0, \pi$ denote bonding (+) and anti-bonding (−) superpositions among the $d\pm$ orbitals after making the gauge transformation $e^{\pm i\delta_b(\mathbf{k})}$. The similarity transform

$$\beta_{d\pm,s}(\mathbf{k}) = e^{\mp i\delta_b(\mathbf{k})} [2^{-1/2} \beta_s(0, \mathbf{k}) \mp 2^{-1/2} \beta_s(\pi, \mathbf{k})] \quad (20)$$

then reduces the Schwinger boson Hamiltonian to

$$H_b = \frac{1}{2} \sum_{k_0=0,\pi} \sum_{\mathbf{k}} \sum_{s=\uparrow,\downarrow} \omega_b(k) [\beta_s^{\dagger}(k) \beta_s(k) + \beta_s(-k) \beta_s^{\dagger}(-k)], \quad (21)$$

with the spectrum

$$\omega_b(k_0, \mathbf{k}) = [\Omega_{\parallel}^2(\mathbf{k}) - \Omega_{\perp}^2(\mathbf{k})]^{1/2} + e^{ik_0} |\Omega'_{\perp}(\mathbf{k})|. \quad (22)$$

The charge-excitation spectrum due to the slave fermions, on the other hand, is obtained directly by the similarity transform

$$f_{d\pm}(\mathbf{k}) = e^{\pm i\delta_f(\mathbf{k})} [2^{-1/2} f(0, \mathbf{k}) \mp 2^{-1/2} f(\pi, \mathbf{k})], \quad (23)$$

where $e^{2i\delta_f(\mathbf{k})}$ denotes the phase factor of the inter-orbital matrix element $\varepsilon_{\perp}(\mathbf{k})$. It yields the diagonal form

$$H_f = \sum_{k_0=0,\pi} \sum_{\mathbf{k}} \varepsilon_f(k) f^{\dagger}(k) f(k) \quad (24)$$

for the slave-fermion Hamiltonian, with spectrum

$$\varepsilon_f(k_0, \mathbf{k}) = \varepsilon_{\parallel}(\mathbf{k}) + e^{ik_0} |\varepsilon_{\perp}(\mathbf{k})|. \quad (25)$$

The low-energy spin and charge excitations that result from ω_b and ε_f will be discussed in detail below.

We must first obtain the mean fields P , Q and R , however. Taking the quantum-thermal average of the constraint against double occupancy (8), and averaging it over the bulk, we get the principal mean-field equation

$$s_0 + \frac{1}{2}(1-x) = \mathcal{N}^{-1} \sum_k (\cosh 2\theta) \left(\frac{1}{2} + n_B[\omega_b(k)] \right), \quad (26)$$

where $\mathcal{N} = 2N_{\text{Fe}}$, and where n_B denotes the Bose-Einstein distribution: $n_B(\omega) = [\exp(\omega/k_B T) - 1]^{-1}$. Next, averaging the definitions of the mean fields (9)-(13) over the bulk yields self-consistent equations

$$Q_n^{\parallel} = \mathcal{N}^{-1} \sum_k \gamma_n(\mathbf{k}) [\cosh 2\theta(\mathbf{k})] \left(\frac{1}{2} + n_B[\omega_b(k)] \right) \quad (n = 1, 2) \quad (27a)$$

$$Q_n^{\perp} = \mathcal{N}^{-1} \sum_k \gamma_n(\mathbf{k}) [\sinh 2\theta(\mathbf{k})] \left(\frac{1}{2} + n_B[\omega_b(k)] \right) \quad (n = 0, 1, 2) \quad (27b)$$

and

$$\begin{aligned} R_1^{\perp}(\hat{\mathbf{n}}) &= \mathcal{N}^{-1} \sum_k (\cos k_n a) e^{ik_0} e^{2i\delta_b(\mathbf{k})} n_B[\omega_b(k)] \quad (n = x, y) \\ R_2^{\perp}(\hat{\mathbf{y}} \pm \hat{\mathbf{x}}) &= \mathcal{N}^{-1} \sum_k (\cos k_{\pm} a) e^{ik_0} e^{2i\delta_b(\mathbf{k})} n_B[\omega_b(k)] \end{aligned} \quad (28)$$

associated with the Schwinger bosons, and it yields self-consistent equations

$$P_n^{\parallel} = \frac{1}{2} \mathcal{N}^{-1} \sum_k \gamma_n(\mathbf{k}) n_F[\varepsilon_f(k)] \quad (n = 1, 2) \quad (29)$$

and

$$\begin{aligned} P_1^{\perp}(\hat{\mathbf{n}}) &= \frac{1}{2} \mathcal{N}^{-1} \sum_k (\cos k_n a) e^{ik_0} e^{2i\delta_f(\mathbf{k})} n_F[\varepsilon_f(k)] \quad (n = x, y) \\ P_2^{\perp}(\hat{\mathbf{y}} \pm \hat{\mathbf{x}}) &= \frac{1}{2} \mathcal{N}^{-1} \sum_k (\cos k_{\pm} a) e^{ik_0} e^{2i\delta_f(\mathbf{k})} n_F[\varepsilon_f(k)] \end{aligned} \quad (30)$$

associated with the slave fermions. Above, n_F denotes the Fermi-Dirac distribution: $n_F(\varepsilon) = (\exp[(\varepsilon - \mu)/k_B T] + 1)^{-1}$, with a chemical potential μ . Let us now assume that

the mean fields R_1^\perp and R_2^\perp are both isotropic, which will be shown to be self consistent. This yields the form

$$\begin{aligned}\varepsilon_\perp(\mathbf{k}) &= 4t_1^\perp(\hat{\mathbf{x}})R_1^\perp[\cos(k_x a) - \cos(k_y a)] \\ &\quad + 4t_2^\perp(\hat{\mathbf{x}} + \hat{\mathbf{y}})R_2^\perp[\cos(k_+ a) - \cos(k_- a)],\end{aligned}\quad (31)$$

for the inter-orbital matrix element experienced by slave fermions, where t_1^\perp is real and where t_2^\perp is pure imaginary. It alternates in sign when \mathbf{k} is rotated by $\pi/2$. This d -wave symmetry implies that both $P_1^\perp(\hat{\mathbf{x}}) + P_1^\perp(\hat{\mathbf{y}}) = \mathcal{N}^{-1} \sum_{\mathbf{k}} e^{ik_0} e^{2i\delta_f(\mathbf{k})} \gamma_1(\mathbf{k}) n_F[\varepsilon_f(k)]$ and $P_2^\perp(\hat{\mathbf{x}} + \hat{\mathbf{y}}) + P_2^\perp(\hat{\mathbf{y}} - \hat{\mathbf{x}}) = \mathcal{N}^{-1} \sum_{\mathbf{k}} e^{ik_0} e^{2i\delta_f(\mathbf{k})} \gamma_2(\mathbf{k}) n_F[\varepsilon_f(k)]$ vanish. Their mean-field equations then reduce to

$$\begin{aligned}P_1^\perp(\hat{\mathbf{x}}) &= \frac{1}{4} \mathcal{N}^{-1} \sum_{\mathbf{k}} e^{ik_0} e^{2i\delta_f(\mathbf{k})} [(\cos k_x a) - (\cos k_y a)] n_F[\varepsilon_f(k)], \\ P_2^\perp(\hat{\mathbf{x}} + \hat{\mathbf{y}}) &= \frac{1}{4} \mathcal{N}^{-1} \sum_{\mathbf{k}} e^{ik_0} e^{2i\delta_f(\mathbf{k})} [(\cos k_+ a) - (\cos k_- a)] n_F[\varepsilon_f(k)],\end{aligned}\quad (32)$$

with opposite signs for the orthogonal links. The latter d -wave symmetry then yields the form

$$\Omega'_\perp(\mathbf{k}) = 8t_1^\perp(\hat{\mathbf{x}})P_1^{\perp*}(\hat{\mathbf{x}})\gamma_1(\mathbf{k}) + 8t_2^\perp(\hat{\mathbf{x}} + \hat{\mathbf{y}})P_2^{\perp*}(\hat{\mathbf{x}} + \hat{\mathbf{y}})\gamma_2(\mathbf{k}) \quad (33)$$

for the inter-orbital matrix element experienced by Schwinger bosons. It has s -wave symmetry, and it is thus consistent with the previous assumptions.

To proceed further, we shall assume that both inter-orbital mean fields for Schwinger bosons R_1^\perp and R_2^\perp are real and positive. This will also be confirmed self-consistently. The slave-fermion matrix elements are then approximated by

$$\varepsilon_\parallel(\mathbf{k}) = \varepsilon_\parallel(0) - t_\parallel |\mathbf{k}|^2 a^2 \quad (34a)$$

$$\varepsilon_\perp(\mathbf{k}) = -[t_\perp \cos(2\phi) + it'_\perp \sin(2\phi)] |\mathbf{k}|^2 a^2 \quad (34b)$$

for \mathbf{k} near zero, where $t_\parallel = 2t_1^\parallel Q_1^\parallel + 4t_2^\parallel Q_2^\parallel$, where $t_\perp = 2t_1^\perp(\hat{\mathbf{x}})R_1^\perp$, and where $t'_\perp = 4t_2^\perp(\hat{\mathbf{x}} + \hat{\mathbf{y}})R_2^\perp/i$ are real hopping amplitudes. Above, ϕ denotes the angle that \mathbf{k} makes with x axis. Henceforth, we shall assume hole bands: $t_\parallel < 0$. The constant energy contours $\epsilon_F = \varepsilon_\parallel(\mathbf{k}) \pm |\varepsilon_\perp(\mathbf{k})|$ then yield Fermi surfaces

$$k_{F\pm}^2(\phi) a^2 = \epsilon'_F / (-t_\parallel \pm [t_\perp^2 \cos^2(2\phi) + t'^2_\perp \sin^2(2\phi)]^{1/2}) \quad (35)$$

at low doping $x \ll 1$, where $\epsilon'_F = \epsilon_F - \varepsilon_\parallel(0)$. These are shown in Fig. 2. The average of the volume of phase space contained by the inner (+) Fermi surface and the outer (-) Fermi surface gives the hole concentration per orbital: $x = (2\pi)^{-2} \int_0^{2\pi} d\phi \sum_\pm \int_0^{k_{F\pm}(\phi)} dk k a^2 / 2$. The resulting angle integral is obtained by applying the residue theorem after making the change of variable $z = e^{4i\phi}$, which yields the relationship

$$4\pi x = \epsilon'_F (-t_\parallel) / (t_\parallel^2 - t_\perp^2)^{1/2} (t_\parallel^2 - t'^2_\perp)^{1/2} \quad (36)$$

between the Fermi energy and the concentration of mobile holes. Next, the intra-layer hopping fields for slave fermions are given by $P_n^\parallel = (2\pi)^{-2} \int_0^{2\pi} d\phi \sum_\pm \int_0^{k_{F\pm}(\phi)} dk k (1 -$

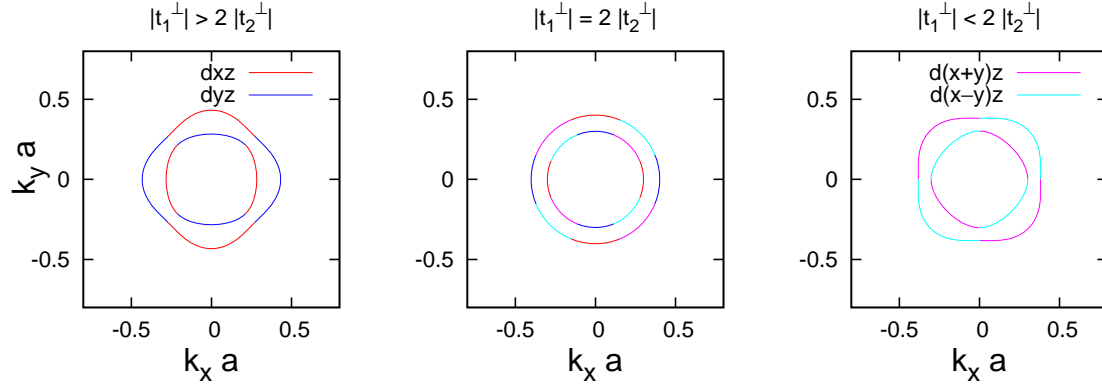


Figure 2. Shown are the hole Fermi surfaces centered at zero 2D momentum. The concentration of holes is universally set to $x = 0.01$, while the hopping matrix elements from left to right are (a) $t_\perp = 0.40(-t_\parallel)$ and $t'_\perp = 0.23(-t_\parallel)$, (b) $t_\perp = 0.28(-t_\parallel)$ and $t'_\perp = 0.28(-t_\parallel)$, and (c) $t_\perp = 0.23(-t_\parallel)$ and $t'_\perp = 0.40(-t_\parallel)$. Above, orbital labels are only approximate near the points on the Fermi surfaces at which they change.

$\frac{n}{4}k^2a^2)a^2/4$ at $x \ll 1$. Performing the integral after the previous change of variable yields the result

$$P_n^\parallel = \frac{1}{2}x - \frac{n\pi}{4}x^2 \frac{t_\parallel^2 - t_\perp^2 t'^2_\perp / t_\parallel^2}{(t_\parallel^2 - t_\perp^2)^{1/2} (t_\parallel^2 - t'^2_\perp)^{1/2}} \quad (37)$$

for these amplitudes. Last, the mean fields for inter-orbital hopping by slave fermions are given by $P_1^\perp(\hat{\mathbf{x}}) = (2\pi)^{-2} \int_0^{2\pi} d\phi \sum_\pm \int_0^{k_{F^\pm}(\phi)} dk k^3 (\mp \cos 2\phi) e^{2i\delta_f(\mathbf{k})} a^4/16$ and by $P_2^\perp(\hat{\mathbf{x}} + \hat{\mathbf{y}}) = (2\pi)^{-2} \int_0^{2\pi} d\phi \sum_\pm \int_0^{k_{F^\pm}(\phi)} dk k^3 (\mp \sin 2\phi) e^{2i\delta_f(\mathbf{k})} a^4/8$ at low hole concentrations, where

$$e^{2i\delta_f(\mathbf{k})} = -\frac{t_\perp \cos(2\phi) + it'_\perp \sin(2\phi)}{[t_\perp^2 \cos^2(2\phi) + t'^2_\perp \sin^2(2\phi)]^{1/2}} \quad (38)$$

is the phase shift at \mathbf{k} near zero. Employing again the change of variable $z = e^{4i\phi}$ in the resulting angle integrals then yields the following expressions for these amplitudes:

$$P_1^\perp(\hat{\mathbf{x}}) = \frac{\pi}{4}x^2 \frac{t_\perp}{t_\parallel} \left(\frac{t_\parallel^2 - t_\perp^2}{t_\parallel^2 - t'^2_\perp} \right)^{1/2}, \quad (39)$$

$$P_2^\perp(\hat{\mathbf{x}} + \hat{\mathbf{y}}) = i\frac{\pi}{2}x^2 \frac{t'_\perp}{t_\parallel} \left(\frac{t_\parallel^2 - t_\perp^2}{t_\parallel^2 - t'^2_\perp} \right)^{1/2}. \quad (40)$$

Substitution into the expression for the inter-orbital matrix element experienced by Schwinger bosons (33) reduces it to

$$\Omega'_\perp(\mathbf{k}) = \pi x^2 R_1^\perp \frac{|2t_1^\perp|^2}{t_\parallel} \left(\frac{t_\parallel^2 - t_\perp^2}{t_\parallel^2 - t_\perp'^2} \right)^{1/2} \gamma_1(\mathbf{k}) + \pi x^2 R_2^\perp \frac{|4t_2^\perp|^2}{t_\parallel} \left(\frac{t_\parallel^2 - t_\perp^2}{t_\parallel^2 - t_\perp'^2} \right)^{1/2} \gamma_2(\mathbf{k}). \quad (41)$$

Observe that the phase factor associated with Schwinger bosons is then $e^{2i\delta_b(\mathbf{k})} = \text{sgn } t_\parallel = -1$ at \mathbf{k} near 0. The principal mean-field equation (26) implies ideal Bose-Einstein condensation (BEC) of the Schwinger bosons into the bottom of the spectrum (22) at 3 momentum $(k_0, \mathbf{k}) = (\pi, 0)$ in the zero-temperature limit. Comparison of (26) with the mean-field equations (27a) and (27b) yields the mean-field values $Q_n^\parallel = s_0$ and $Q_n^\perp = s_1$, in the large- s_0 limit, where $s_1 = s_0 \tanh 2\theta(0) = [\Omega_\perp(0)/\Omega_\parallel(0)]s_0$. Ideal BEC necessarily requires $\omega_b(\pi, 0) = 0$. This yields ultimately that $\tanh 2\theta(0) = (1 + [\Omega'_\perp(0)/\Omega_\perp(0)]^2)^{-1/2}$. Inter-orbital hopping therefore diminishes the antiferromagnetic order in the hidden half metal state: $s_1 < s_0$. Notice, however, that the correction is small and of order x^4 ! Last, ideal BEC implies a unique mean-field amplitude $R_n^\perp = s_2$ by meanfield equations (28), where $s_2 = s_0 / \cosh 2\theta(0) = [|\Omega'_\perp(0)|/\Omega_\perp(0)] / (1 + [\Omega'_\perp(0)/\Omega_\perp(0)]^2)^{1/2}$. Observe now that the latter ratio of frequencies takes the form $|\Omega'_\perp(0)|/\Omega_\perp(0) = A_0(s_2/s_0s_1)$ as $x \rightarrow 0$, in which case $s_1 \rightarrow s_0$. Here, A_0 is a positive constant that is small compared to unity at low hole concentration. Substituting this form into the previous definition of s_2 yields only the trivial solution $s_2 = 0$. We therefore conclude that inter-orbital hopping is dynamically suppressed in the present Schwinger-boson-slave-fermion mean-field theory for the hidden half-metal state at large electron spin s_0 and low hole concentration. In particular, Eqs. (39) and (40) imply that both the inter-orbital fields P_n^\perp and R_n^\perp are null.

Dynamical suppression of inter-orbital hopping at large- s_0 implies a null inter-orbital hopping matrix element for Schwinger bosons by Eq. (41): $\Omega'_\perp(\mathbf{k}) = 0$. Inspection of the spectrum for Schwinger bosons (22) then yields that it disperses as

$$\omega_b(k_0, \mathbf{k}) = v_0 |\mathbf{k}| \quad \text{near } \mathbf{k} = 0, \quad (42)$$

where

$$v_0 = 2s_0 a (1-x)^2 ([J_1^\perp - \bar{J}_1^\parallel(x) + 2J_2^\perp - 2\bar{J}_2^\parallel(x)] \cdot [\frac{1}{2}J_0 + 2J_1^\perp + 2J_2^\perp])^{1/2} \quad (43)$$

is the longitudinal spin-wave velocity, with $\bar{J}_n^\parallel(x) = J_n^\parallel + (1-x)^{-2} s_0^{-1} t_n^\parallel x$ for $n = 1, 2$. At \mathbf{k} near cSDW wavenumbers $(\pi/a, 0)$ and $(0, \pi/a)$, the spectrum for Schwinger bosons (22) disperses anisotropically as

$$\omega_b(k_0, \mathbf{k}) = [\Delta_{cSDW}^2 + v_0^2(k_l - \pi/a)^2 + v_0^2(k_t/\gamma_{cSDW})^2]^{1/2}, \quad (44)$$

with a spin gap

$$\Delta_{cSDW} = (1-x)^2 (2s_0) [(4J_2^\perp - J_{0c})(J_0 - J_{0c})]^{1/2}, \quad (45)$$

and with an anisotropy parameter

$$\gamma_{cSDW} = ([2\bar{J}_2^\parallel(x) + 2J_2^\perp + \bar{J}_1^\parallel(x) + J_1^\perp] / [2\bar{J}_2^\parallel(x) + 2J_2^\perp - \bar{J}_1^\parallel(x) - J_1^\perp])^{1/2}, \quad (46)$$

which is greater than unity. Here, the critical Hund's Rule coupling at which $\Delta_{cSDW} \rightarrow 0$ is

$$-J_{0c} = 2(J_1^\perp - J_1^\parallel) - 4J_2^\parallel - (1-x)^{-2}s_0^{-1}2t_\parallel x. \quad (47)$$

The hidden half-metal is stable at weak to moderate Hund's Rule coupling $-J_0 < -J_{0c}$. Equation (47) therefore implies that intra-orbital hole hopping stabilizes the hidden half-metal state for hole bands, $t_\parallel < 0$. (See Fig. 1.) We conclude that the hidden half-metal is robust with respect to the presence of inter-orbital hopping within the present Schwinger-boson-slave-fermion mean-field theory.

Finally, returning to the generic unoptimized mean-field theory, the inversion of the similarity transform (23) yields slave-fermion states that are annihilated by

$$f(k_0, \mathbf{k}) = \frac{e^{+i\delta_f(\mathbf{k})}}{2^{1/2}} f_{d-}(\mathbf{k}) + e^{ik_0} \frac{e^{-i\delta_f(\mathbf{k})}}{2^{1/2}} f_{d+}(\mathbf{k}). \quad (48)$$

Their corresponding Wannier wave functions then depend on the azimuthal angle ϕ' about each iron atom as $\cos[\phi' - \delta_f(\mathbf{k})]$ in the even channel and as $\sin[\phi' - \delta_f(\mathbf{k})]$ in the odd channel. Figure 2 depicts slave-fermion Fermi surfaces (35) at low doping $x = 0.01$. Dynamical suppression of inter-orbital hopping implies that the matrix element for inter-orbital hopping of slave fermions (18) is null, however. The inner and outer Fermi surface hole pockets depicted by Fig. 2 must therefore collapse into two degenerate circular Fermi surface hole pockets at low doping, $x \ll 1$, at large spin s_0 . We believe that this effect is due to the inability of the two-orbital t - J model (1) to “erase” strings of overturned spins that result from inter-orbital hole hopping in the classical limit, at large spin s_0 [26][27]. As we will see in the next section, this limiting result persists for true electron spin $s_0 = 1/2$ in certain cases.

3.2. Spinwaves

We shall now determine the spin excitations of the hidden half metal by directly computing the dynamical spin-spin correlation function from the Schwinger-boson-slave-fermion mean-field theory. First, we identify the true ($k_0 = 0$) versus the hidden ($k_0 = \pi$) spin at each iron atom i : $\mathbf{S}_i(k_0) = \mathbf{S}_{i,d-} + e^{ik_0} \mathbf{S}_{i,d+}$. Consider then the transverse dynamical spin-spin correlation function $\langle \mathbf{S}(k_0) \cdot \mathbf{S}'(k_0) \rangle^\perp = \frac{1}{2} \langle S^+(k_0) S'^-(k_0) + S^-(k_0) S'^+(k_0) \rangle$ at space-time points (\mathbf{r}, t) and (\mathbf{r}', t') . Averaging the slave-fermion dynamics over the bulk, we obtain the form

$$\begin{aligned} \langle \mathbf{S}(k_0) \cdot \mathbf{S}'(k_0) \rangle^\perp_{\mathbf{k}, \omega} &= (1-x)^2 \frac{\hbar^2}{2} \sum_{\alpha=0,1} \sum_{\beta=0,1} e^{ik_0(\alpha-\beta)} \cdot \\ &\quad \cdot [G_{\alpha,\beta}^{(b)} * G_{\alpha,\beta}^{(b)*} + F_{\alpha,\beta}^{(b)} * F_{\alpha,\beta}^{(b)*}]_{\mathbf{k}, \omega}, \end{aligned} \quad (49)$$

for its Fourier transform, where $iG_{\alpha,\beta}^{(b)}(\mathbf{r}_i, t; \mathbf{r}_j, t') = \langle b_{i,\alpha,s}(t) b_{j,\beta,s}^\dagger(t') \rangle$ and $iF_{\alpha,\beta}^{(b)}(\mathbf{r}_i, t; \mathbf{r}_j, t') = \langle b_{i,\alpha,s}(t) b_{j,\beta,\bar{s}}(t') \rangle$ are the regular and the anomalous Greens functions for the Schwinger bosons, and where the notation $f * g$ denotes a convolution in frequency and momentum. Above, we use the index 0 and 1 for the orbitals $d-$ and $d+$.

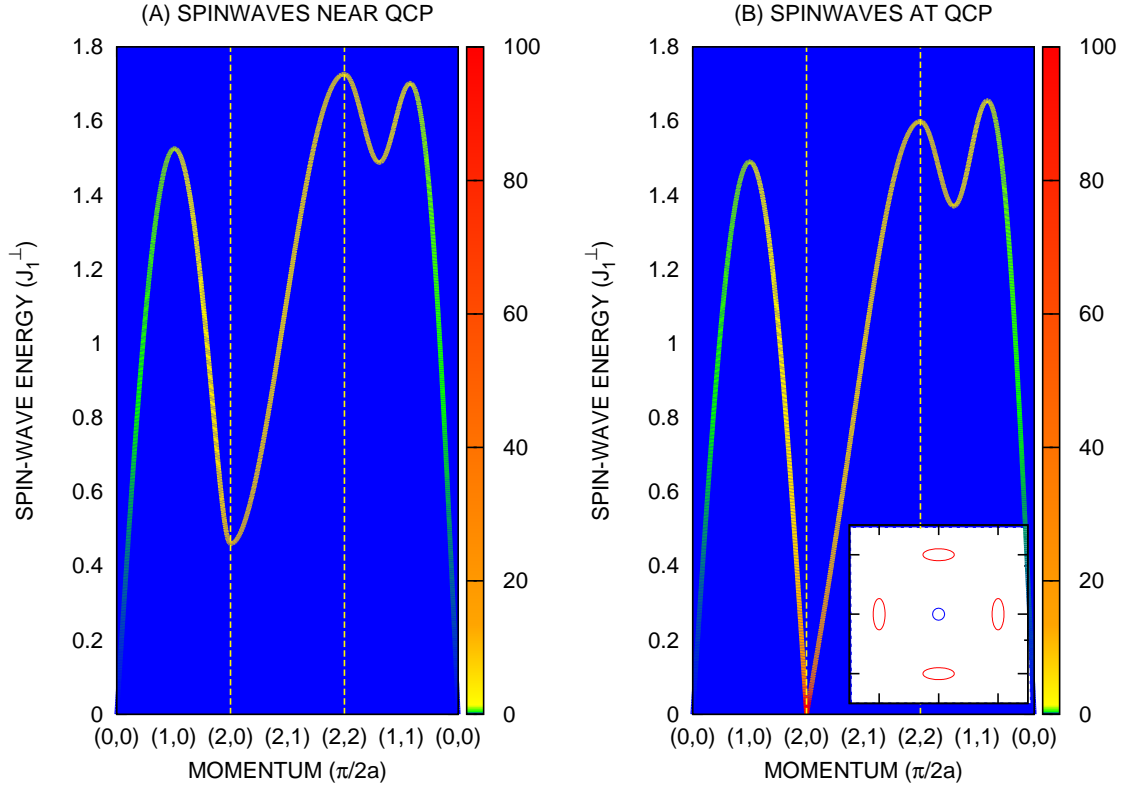


Figure 3. The mean-field result for the imaginary part of the dynamical spin response function in the zero-temperature-large- s_0 limit, Eqs. (51) and (52), is evaluated with the following set of parameters: $J_1^{\parallel} = 0$, $J_1^{\perp} > 0$, $J_2^{\parallel} = 0.3 J_1^{\perp} = J_2^{\perp}$, $t_1^{\parallel} = -5J_1^{\perp}$, $t_2^{\parallel} = 0$, $x = 0.01$, and $s_0 = 1/2$. Dynamical suppression of inter-orbital hopping is presumed. The Hund's Rule coupling is set to $-J_0 = -J_{0c} - 0.1J_1^{\perp}$ just off the QCP in panel (A), while it is set to the critical value $-J_{0c}$ in panel (B). Low-energy contours are displayed in the inset.

Also, henceforth in this subsection, we shall identify $k_0 = 0$ and π with the respective labels $+$ and $-$. After substitution of the Bogoliubov transformation (19a,b) and of the similarity transform (20), a standard summation of the Matsubara frequencies in the convolution yields the following Auerbach-Arovas expression for the dynamical spin correlator at $T > 0$ [32]:

$$\begin{aligned}
 i\langle \mathbf{S}(\pm) \cdot \mathbf{S}'(\pm) \rangle|_{\mathbf{k},\omega}^{\perp} &= \frac{\hbar^2 (1-x)^2}{4 \mathcal{N}} \sum_{q_0=+,-} \sum_{\mathbf{q}} \left\{ (1 + \cosh [2\theta(\mathbf{q}) \mp 2\theta(\mathbf{q} - \mathbf{k})]) \cdot \right. \\
 &\quad \cdot \sum_{\nu=-\omega,+\omega} \frac{n_B[\omega_b(q_0, \mathbf{q})] - n_B[\omega_b(q_0 \pm, \mathbf{q} - \mathbf{k})]}{\nu - \omega_b(q_0, \mathbf{q}) + \omega_b(q_0 \pm, \mathbf{q} - \mathbf{k})} + \\
 &\quad + (1 - [\cosh 2\theta(\mathbf{q})][\cosh 2\theta(\mathbf{q} - \mathbf{k})]) \cdot \\
 &\quad \cdot \sum_{\nu=-\omega,+\omega} \frac{n_B[\omega_b(q_0, \mathbf{q})] + n_B[\omega_b(q_0 \pm, \mathbf{q} - \mathbf{k})]}{\nu - \omega_b(q_0, \mathbf{q}) - \omega_b(q_0 \pm, \mathbf{q} - \mathbf{k})} + \\
 &\quad \left. \pm [\sinh 2\theta(\mathbf{q})][\sinh 2\theta(\mathbf{q} - \mathbf{k})] \right\}.
 \end{aligned}$$

$$\cdot \sum_{\nu=-\omega, +\omega} \frac{n_B[\omega_b(q_0, \mathbf{q})] + n_B[\omega_b(q_0 \mp, \mathbf{q} - \mathbf{k})]}{\nu - \omega_b(q_0, \mathbf{q}) - \omega_b(q_0 \mp, \mathbf{q} - \mathbf{k})} \Big\}. \quad (50)$$

When computing $q_0 \pm$ above, we use the multiplication table $\pm\pm = +$ and $\mp\pm = -$. The property $\omega_b(q_0, \mathbf{q}) = \omega_b(q_0, -\mathbf{q})$ displayed by the spectrum for Schwinger bosons (22) was exploited to obtain the reduced expression (50). Expression (50) can be used to show that $(2\pi)^{-1} \int_{-\infty}^{+\infty} d\omega \langle \mathbf{S}(+) \cdot \mathbf{S}'(+) \rangle|_{\mathbf{k}, \omega}^\perp = 0$ at $\mathbf{k} = 0$. This is consistent with a spin-singlet hidden-order antiferromagnetic state inside the subspace where $\sum_i \sum_\alpha S_{z,i,\alpha} = 0$: $\langle |\sum_i \sum_\alpha \mathbf{S}_{i,\alpha}|^2 \rangle = 0$. Expression (50) for the dynamical spin correlator is easily evaluated in the zero-temperature limit, where ideal BEC of the Schwinger bosons into the $(q_0, \mathbf{q}) = (-, 0)$ ground state occurs (26). At large s_0 , in particular, the third and last term of this expression is given by

$$i \langle \mathbf{S}(-) \cdot \mathbf{S}'(-) \rangle|_{\mathbf{k}, \omega}^{\perp, 3} = \pi^{-1} A_3(-, \mathbf{k}) ([\omega_b(-, \mathbf{k}) - \omega]^{-1} + [\omega_b(-, \mathbf{k}) + \omega]^{-1}),$$

for the case of hidden magnetic order, where the poles in frequency have spectral weight

$$A_3(-, \mathbf{k}) = \pi(1-x)^2 (s_0/2) \hbar^2 [\tanh 2\theta(0)] [\Omega_\perp(\mathbf{k})/\omega_b^{(0)}(\mathbf{k})],$$

with $\omega_b^{(0)}(\mathbf{k}) = [\Omega_\parallel^2(\mathbf{k}) - \Omega_\perp^2(\mathbf{k})]^{1/2}$. It reveals a Goldstone mode at $\mathbf{k} = 0$. Ideal BEC yields poles in frequency that exhibit a spin gap in the hidden channel $(-)$ at $\mathbf{k} = 0$ from the first and second terms of expression (50), on the other hand. The present mean-field theory for the hidden half-metal state therefore generally shows long-range antiferromagnetic order across the $d+$ and $d-$ orbitals, which is consistent with Goldstone's theorem.

At large electron spin s_0 , the true self-consistent mean-field theory dynamically suppresses inter-orbital hopping, however. This leads to Schwinger bosons with degenerate spectra: $\omega_b(q_0, \mathbf{k}) = \omega_b^{(0)}(\mathbf{k})$ for $q_0 = +, -$. Expression (50) in conjunction with ideal BEC then yields the result[18]

$$i \langle \mathbf{S}(\pm) \cdot \mathbf{S}'(\pm) \rangle|_{\mathbf{k}, \omega}^\perp = \pi^{-1} A(\pm, \mathbf{k}) ([\omega_b^{(0)}(\mathbf{k}) - \omega]^{-1} + [\omega_b^{(0)}(\mathbf{k}) + \omega]^{-1}), \quad (51)$$

where the poles in frequency have spectral weight

$$A(\pm, \mathbf{k}) = \pi(1-x)^2 s_0 \hbar^2 [\Omega_\mp(\mathbf{k})/\Omega_\pm(\mathbf{k})]^{1/2}. \quad (52)$$

Here, $\Omega_\pm = \Omega_\parallel \pm \Omega_\perp$. The above dynamical spin correlator coincides with the transverse spin susceptibility, $\chi_\perp(k, \omega)$, in the present zero-temperature limit by the fluctuation-dissipation theorem. Notice that the nature of the spectral weights (52) above implies the existence of hidden $(-)$ spin waves near zero 2D momentum with a spectrum (42), as well as true $(+)$ spin waves near cSDW momenta with a spectrum (44) [18]. We conclude that the hidden half-metal state shows strict long-range antiferromagnetic order across the $d+$ and $d-$ orbitals of the iron atoms in the presence of inter-orbital hopping.

The true spin excitations $(+)$ predicted by the dynamical spin susceptibility (51) near the quantum-critical point are shown graphically by Fig. 3 for a set of parameters that is applicable to iron-pnictide high-temperature superconductors. Notice the spin gap (45) that exists at cSDW wavenumbers $\mathbf{k}_{cSDW} = (\pi/a)\hat{x}$ and $(\pi/a)\hat{y}$. It collapses

to zero at a critical Hund's Rule coupling $-J_{0c}$ of moderate strength (47). This strongly suggests that the hidden half metal state gives way to a cSDW metal phase[33] that shows strict long-range cSDW order at the QCP that separates the two phases. The critical cSDW metal has a low ordered moment because of proximity to the hidden half metal state.

3.3. Fermi Surfaces

We shall now obtain the electronic structure of the hidden half metal state by computing the one-electron propagator directly from the Schwinger-boson-slave-fermion mean-field theory for the two-orbital t - J model. It is given by the convolution of the propagator for Schwinger bosons with the propagator for slave fermions: $iG(\mathbf{k}, \omega) = \sum_{\alpha=d-, d+} G_{\alpha, \alpha}^{(b)} * G_{\alpha, \alpha}^{(f)*} |_{\mathbf{k}, \omega}$, where $iG_{\alpha, \beta}^{(f)}(\mathbf{r}_i, t; \mathbf{r}_j, t') = \langle f_{i, \alpha}(t) f_{j, \beta}^\dagger(t') \rangle$. A standard summation of Matsubara frequencies yields the expression[18]

$$G(\mathbf{k}, \omega) = \sum_{k_0=0, \pi} \frac{1}{\mathcal{N}} \sum_q \left([\cosh \theta(\mathbf{q})]^2 \frac{n_B[\omega_b(q)] + n_F[\varepsilon_f(q - k)]}{\omega - \omega_b(q) + \varepsilon_f(q - k)} + [\sinh \theta(\mathbf{q})]^2 \frac{\bar{n}_B[\omega_b(q)] + \bar{n}_F[\varepsilon_f(q - k)]}{\omega + \omega_b(q) + \varepsilon_f(q - k)} \right). \quad (53)$$

Above, $\bar{n}_F(\varepsilon) = (\exp[(\mu - \varepsilon)/k_B T] + 1)^{-1}$ is the time-reversed Fermi-Dirac distribution. All of the Schwinger bosons condense into the lowest-energy state at 3 momentum $(q_0, \mathbf{q}) = (\pi, 0)$ as $T \rightarrow 0$ by the principal meanfield equation (26). This results in the following coherent contribution to the electronic spectral function at zero temperature and at large s_0 :

$$\text{Im } G_{\text{coh}}(\mathbf{k}, \omega) = s_0 \pi \sum_{k_0=0, \pi} \delta[\omega + \varepsilon_f(k_0, \mathbf{k})]. \quad (54)$$

In the case of the unoptimized generic mean-field theory, it reveals inner and outer hole Fermi surfaces centered at zero 2D momentum that are depicted by Fig. 2. These collapse into doubly-degenerate circular hole pockets in the self-consistent mean-field theory at large s_0 , where inter-orbital hopping is dynamically suppressed. The contribution due to the Fermi-Dirac terms in the expression above represent incoherent excitations in the electronic structure. At energies ω below the electronic Fermi level, the pole in the second term of expression (53) above represents the combination of a hole excitation, $\varepsilon_f > \mu$, with a spinwave, $\omega_b > 0$. This composite excitation therefore shows a gap (45) at cSDW momenta, Δ_{cSDW} . Notice that copies of the previous inner and outer Fermi surfaces now centered at cSDW wavenumbers $(\pi/a)\hat{\mathbf{x}}$ and $(\pi/a)\hat{\mathbf{y}}$ exist at the QCP because of the collapse of the spin gap there: $\Delta_{\text{cSDW}} \rightarrow 0$. (See Fig. 3.) This is a spin-density wave nesting mechanism in reverse, where low-energy spinwaves centered at cSDW momenta produce nested Fermi surfaces! The incoherent contribution due to the first term in expression (53) above vanishes in the zero-temperature limit at energies ω below the electronic Fermi level. Last, the ratio of the incoherent spectral function integrated over momentum in the vicinity $\mathbf{k} = 0$ or $(\pi/a)\hat{\mathbf{x}}(\hat{\mathbf{y}})$ compared to the coherent

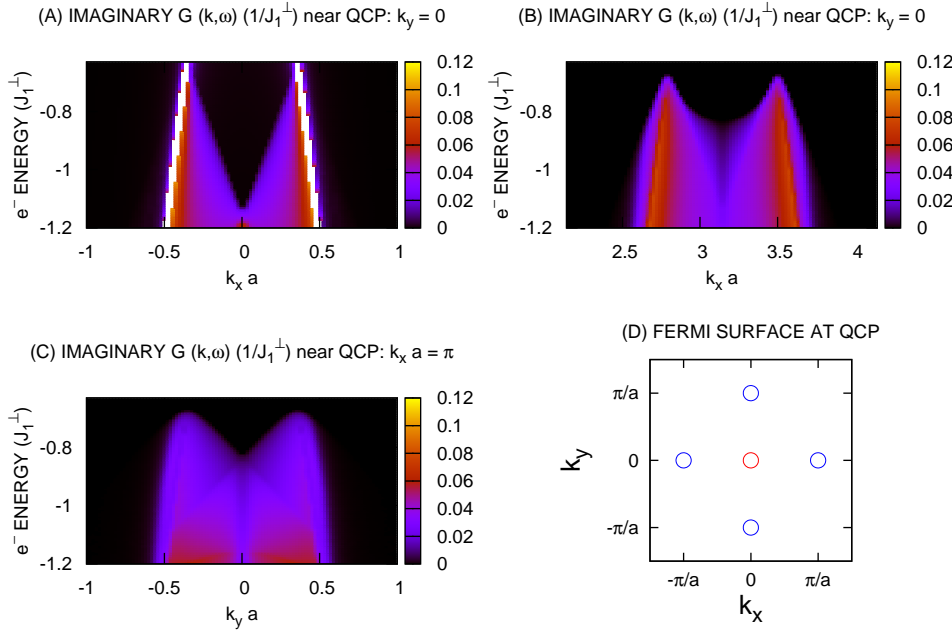


Figure 4. Shown is the imaginary part of expression (53) with the parameter set that is listed in the previous caption to Fig. 3, but at Hund's Rule coupling $-J_0 = -J_{0c} - 0.001J_1^\perp$. The electron energy $\hbar\omega$ is measured with respect to the top of the hole band, $-\varepsilon_\parallel(0)$.

counterpart is $\sum_{\mathbf{k}}' \text{Im} G_{\text{inc}}(\mathbf{k}, \omega) / \sum_{\mathbf{k}} \text{Im} G_{\text{coh}}(\mathbf{k}, \omega) = (\gamma/4\pi s_0) \cdot [(\Delta\omega - \Delta)\Omega_\parallel / (v_0/a)^2]$. Here, $\Delta\omega$ measures how far in energy the hole lies below the Fermi level, $\Delta = 0$ in the region of 2D momentum centered at $\mathbf{k} = 0$, and $\Delta = \Delta_{cSDW}$ in the region of 2D momentum centered at \mathbf{k}_{cSDW} . It is assumed that $\Delta\omega > \Delta$. Also, γ is the anisotropy parameter of the spinwave dispersion in question. (See fig. 3a.)

We will now evaluate the former incoherent contribution to the spectral function in the large- s_0 limit in the vicinity of the QCP, where Δ_{cSDW} is small, at energies just below the Fermi level. As predicted by the mean-field theory, we shall assume that inter-orbital hopping is dynamically suppressed: $\varepsilon_f(k_0, \mathbf{k}) = \varepsilon_\parallel(\mathbf{k})$. The hole Fermi surfaces centered at zero 2D momentum (Fig. 2) then reduce to two degenerate circular hole pockets at low doping. The previous long-wavelength approximations for the spinwave dispersion near zero 2D momentum (42) and near cSDW momenta (44) are then valid. Also valid is the long-wavelength approximation for the dispersion of the slave fermions (34a), with $t_\parallel < 0$. The imaginary part of the poles in the first (−) and second (+) terms of Eq. (53) enforce energy conservation: $-\omega = \pm\omega_b^{(0)}(\mathbf{q}) + \varepsilon_\parallel(\mathbf{q} - \mathbf{k})$. Taking the product of the two poles and enforcing energy conservation yields $0 = [\omega + \varepsilon_\parallel(\mathbf{q} - \mathbf{k})]^2 - [\omega_b^{(0)}(\mathbf{q})]^2$. Substituting in the long-wavelength approximations for the spectra of the Schwinger bosons and of the slave fermions then yields a quartic equation for $|\mathbf{q}|$. Its roots can be obtained analytically. We thus computed the incoherent (Fermi-Dirac) contribution to the electronic structure $\text{Im} G_{\text{inc}}(\mathbf{k}, \omega)$ in the thermodynamic limit from expression (53)

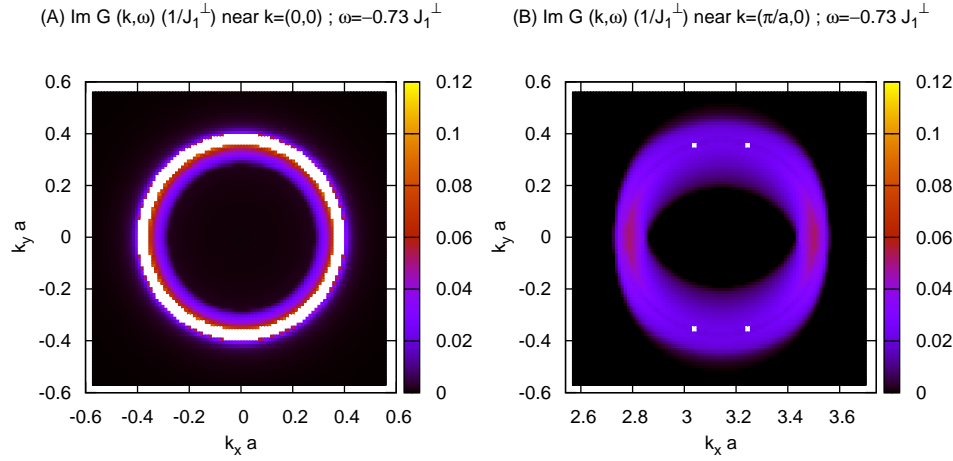


Figure 5. Shown is the imaginary part of expression (53) near the QCP at fixed energy just below the Fermi level, with the parameter set that is listed in the previous caption to Fig. 4.

by integrating the δ -function that enforces energy conservation over radial momentum $|\mathbf{q}|$ analytically, and by performing the remaining angular integral numerically.

Figure 4 compiles the net electronic structure that is predicted by the present Schwinger-boson-slave-fermion mean-field theory. It is predominantly hole-type about zero 2D momentum because of the coherent contribution (54), which is independent of the Fermi level. Fig. 4a also displays an electron-type “V” that separates purple from black, however. It meets the coherent hole band at the Fermi level, and its slope coincides with the longitudinal spin-wave velocity v_0 . Figures 4b and 4c exhibit the energy gap below the Fermi level, Δ_{cSDW} , that exists at wavenumbers near $(\pi/a)\hat{\mathbf{x}}$. A mix of electron and hole structure exists here at electron energies below the gap. The slope of the electron-type “V” that separates pink from purple in Fig. 4b also coincides with the longitudinal spin-wave velocity v_0 , whereas the slope of the electron-type “V” that separates purple from black in Fig. 4c coincides with the transverse spin-wave velocity v_0/γ_{cSDW} . We conclude that the group velocity of the electron-type dispersion at 2D momentum near a point on one of the Fermi surfaces centered at a cSDW wavenumber $(\pi/a, 0)$ or $(0, \pi/a)$ is equal to the *spin-wave velocity* at the former momentum. Figure 4b also exhibits hole dispersion that follows the band $\omega = -\varepsilon_\parallel[\mathbf{k} - (\pi/a)\hat{\mathbf{x}}]$, however. Its origin is the divergence of the coherence factor $\sinh^2 \theta(\mathbf{q})$ in Eq. (53) as the spin-wave frequency $\omega_b^{(0)}(\mathbf{q})$ begins to vanish at $\mathbf{q} = (\pi/a)\hat{\mathbf{x}}(\hat{\mathbf{y}})$ near the QCP. Figure 4c shows that this effect is much less prominent along the transverse scan in 2D momentum. Last, Fig. 5 displays the same electronic structure as Fig. 4, but at a constant energy that lies

halfway between the Fermi level and the minimum of the electron-type “V” dispersion at sSDW momenta. Panel (B) shows that traces of the hole-type dispersion centered at these momenta exist along the longitudinal (k_x) axes.

4. Exact Diagonalization and Conjecture

The previous Schwinger-boson-slave-fermion meanfield theory for the two-orbital t - J model (1) predicts that inter-orbital hopping is dynamically suppressed in the hidden half-metal state at large electron spin s_0 . Does this result persist for true electron spin, $s_0 = 1/2$? Below, we will see that it does indeed persist when inter-orbital hopping is purely along next-nearest neighbors, while coherent inter-orbital hole propagation is possible in the opposite case where inter-orbital hopping is purely along nearest neighbors.

We have obtained the exact low-energy spectrum of the two-orbital t - J model (1) for $4 \times 4 \times 2$ local spin-1/2 moments plus one mobile hole by computer calculation. Each quantum state is specified by the combination of a spin background over all of the $4 \times 4 \times 2$ sites, confined to the subspace with total spin $S_z = 0$, and one hole location at down-spin sites in the spin background. The Heisenberg-exchange and Hund-exchange terms in the t - J model Hamiltonian (1) reduce to permutations of the spin backgrounds, and these are stored in memory. The matrix elements for correlated hopping terms in (1) are computed directly at each application of the Hamiltonian operator, on the other hand. Periodic boundary conditions are imposed, and translation and reflection symmetries on the $4 \times 4 \times 2$ lattice are exploited in order to reduce the dimension of the Hilbert space. Global swap of the orbitals, $P_{d\bar{d}}$, is included in the list of symmetry operations at the extreme where inter-orbital next-nearest neighbor hopping is suppressed: $t_2^\perp = 0$. For example, exploiting reflections about both principal axes of the 4×4 square lattice of iron atoms brings down the dimension of the Hilbert space to 75,624,211 states in such case at zero-momentum and even reflection parities. The low-energy states of the resulting block-diagonal Hamiltonian are obtained by employing the Lanczos technique[34]. We use the ARPACK subroutine library for this purpose[35], in which case the Hamiltonian operation $|\psi'\rangle = H|\psi\rangle$ is accelerated by exploiting parallel threads with OpenMP directives.

Figures 6, 7 and 8 display the evolution of the low-energy spectrum of one mobile hole in a 4×4 lattice of spin-1 iron atoms with the strength of the Hund’s Rule coupling, $-J_0$. We chose the following set of Heisenberg exchange coupling constants and hopping matrix elements: $J_1^\parallel = 0$, $J_1^\perp > 0$, $J_2^\parallel = 0.3J_1^\perp = J_2^\perp$, $t_1^\parallel = -5J_1^\perp$, $t_1^\perp(\hat{x}) = -2J_1^\perp$, $t_1^\perp(\hat{y}) = +2J_1^\perp$, and $t_2^\parallel = 0 = t_2^\perp$. Recall that global swap of the orbitals, $P_{d\bar{d}}$, is then an exact symmetry. (See the end of section 2.) Also, the mean-field result (47) then predicts a quantum critical point at $J_0 = -0.8J_1^\perp$ in the thermodynamic limit ($x = 0$) that separates a hidden half-metal state at weak Hund’s Rule coupling from a cSDW at strong Hund’s Rule coupling. Figure 6 displays the exact spectrum in the absence of Hund’s Rule. Red and blue points denote states that are respectively even and odd under

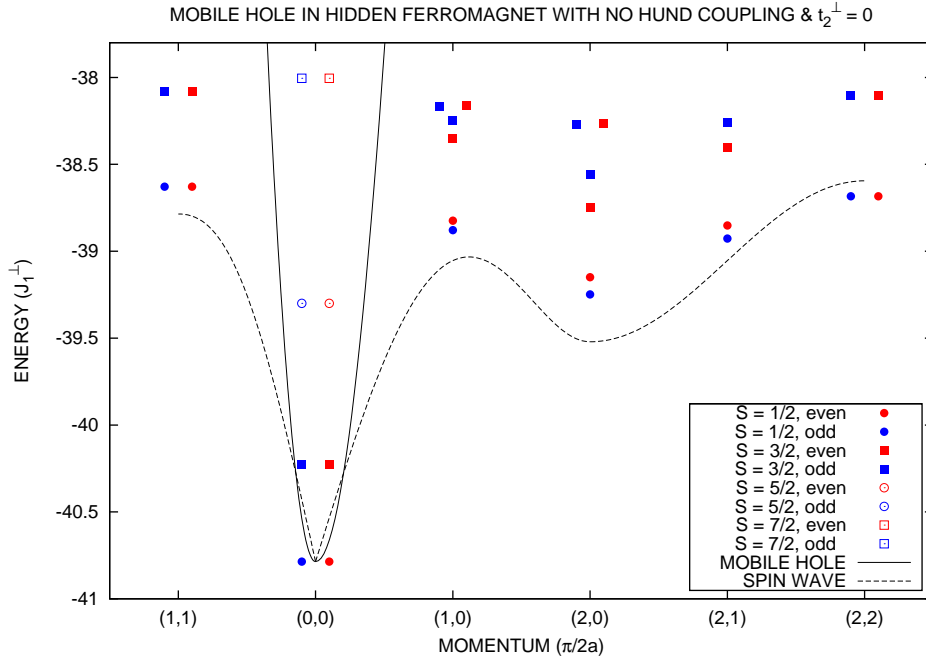


Figure 6. Shown is the low-energy spectrum of the two-orbital t - J model, Eq. (1), over a $4 \times 4 \times 2$ lattice with one hole, in the absence of Hund's Rule: $J_0 = 0$. The remaining parameters are $J_1^\parallel = 0$, $J_1^\perp > 0$, $J_2^\parallel = 0.3J_1^\perp = J_2^\perp$, $t_1^\parallel = -5J_1^\perp$, $t_1^\perp(\hat{x}) = -2J_1^\perp$, $t_1^\perp(\hat{y}) = +2J_1^\perp$, and $t_2^\parallel = 0 = t_2^\perp$. A comparison with the hole spectrum, $\varepsilon_f(k) = \varepsilon_\parallel(\mathbf{k})$, and with the spin-wave spectrum, $\omega_b(k) = \omega_b^{(0)}(\mathbf{k})$, at large s_0 and $x = 0$ is also shown. Henceforth, some points on the spectrum are artificially moved slightly off their quantized values along the momentum axis for the sake of clarity.

$P_{d\bar{d}}$. The spectrum is consistent with a hidden half metal. In particular, the lowest-energy states at fixed momentum carry spin-1/2 and they are nearly doubly degenerate. Furthermore, their dispersion agrees with that predicted by the previous mean-field theory (22) for the low-energy spin-wave excitations of the hidden half-metal state. Finally, the spin-1/2 states in Fig. 6 are well separated from the next excited states at fixed momentum, which carry spin-3/2. This observation is again consistent with well-defined spinwave excitations like those predicted by the dynamical spin susceptibility (51) of the Schwinger-boson-slave-fermion mean-field theory.

Figure 7 shows how the spin-1/2 state at cSDW wavenumber $(\pi/a)\hat{x}$ with odd parity under $P_{d\bar{d}}$, in the absence of Hund's Rule, comes down in energy to become degenerate with the zero-momentum doubly-degenerate groundstate at a critical Hund's Rule coupling of $J_{0c} = -1.73J_1^\perp$. We have measured the expectation value for *local* orbital swap at the hole iron site, $P_{d\bar{d}}(\circ)$. It has eigenvalues +1 and -1, which correspond to a hole with $3d_{xz}$ and with $3d_{yz}$ orbital character, respectively. Table 1 lists the corresponding expectation value over the groundstate at cSDW wavenumber $(\pi/a)\hat{x}$, $\langle P_{d\bar{d}}(\circ) \rangle = -0.47$, which means that the hole has 74% $3d_{yz}$ orbital character. We note that turning off inter-orbital hopping entirely results in a somewhat higher critical Hund's Rule coupling of [18] $J_{0c} = -2.27J_1^\perp$. This dependence on inter-orbital hopping

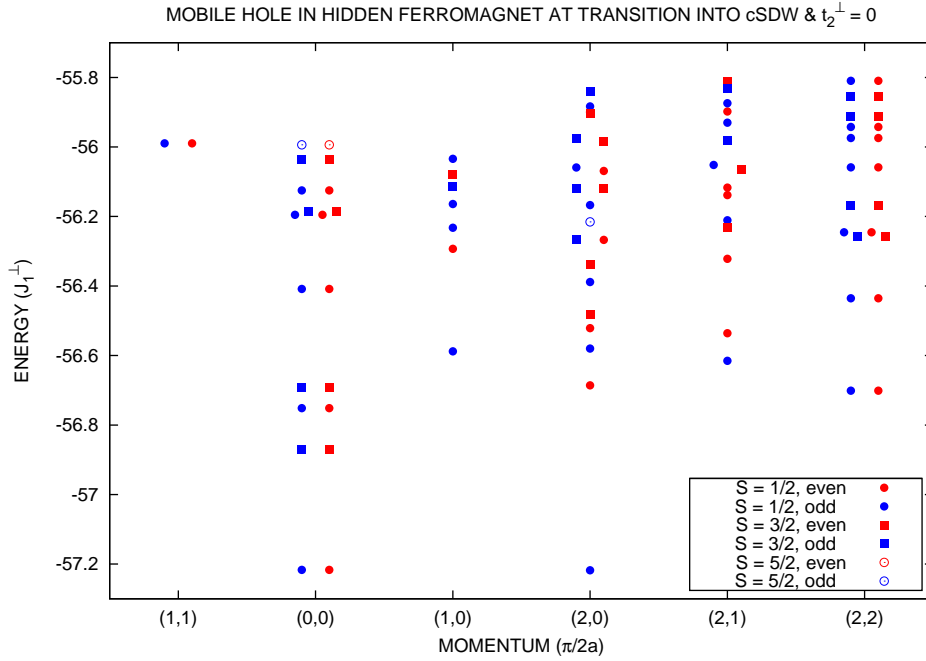


Figure 7. The low-energy spectrum of the two-orbital t - J model with one hole roaming over a $4 \times 4 \times 2$ lattice is displayed at the QCP that separates the cSDW from the hidden half-metal state: $J_{0c} = -1.733J_1^\perp$. The remaining set of parameters are listed in the previous caption to the Fig. 6.

should be compared to the mean-field result (47), which predicts no dependence at all. The dispersion of the low-energy spin-1/2 states shown in Fig. 7 resembles the mean-field prediction for the dispersion of critical spin-wave excitations shown in Fig. 3. The former states are also well separated from the next excited state at fixed momentum. This again is consistent with the mean-field prediction (51) of well-defined spin-wave excitations at the QCP. Finally, the ordered moment for antiferromagnetic order across the $d+$ and $d-$ orbitals that characterizes the hidden half metal and for the cSDW is defined by $\boldsymbol{\mu}(k) = [2\mu_B/(N_{\text{Fe}} - \frac{1}{2})] \sum_{\alpha=0}^1 \sum_i e^{i(k_0\alpha + \mathbf{k} \cdot \mathbf{r}_i)} \mathbf{S}_{i,\alpha}$, with respective 3-momenta $k = (\pi, 0, 0)$ and $k = (0, \pi/a, 0)$. Table 1 lists the auto-correlation of each over the groundstate at zero 2D momentum: $\langle \boldsymbol{\mu}(k) \cdot \boldsymbol{\mu}(-k) \rangle_0$. They are given in units of the ordered moment of the ferromagnetic state, $k = (0, 0, 0)$, over the $4 \times 4 \times 2$ lattice: $\mu_{\text{Fe}}^2 = (33/31)(2\mu_B)^2$. Notice that μ_{cSDW} remains small at the QCP, at zero 2D momentum, which is consistent with neutron diffraction studies in iron-pnictide systems[7]. Notice also that μ_{hFM} remains sizeable at the quantum critical point, at zero 2D momentum, which indicates that hidden half metal character persists there.

Last, Fig. 8 displays the exact low-energy spectrum of a true 4×4 lattice of spin-1 iron atoms with one mobile hole. In particular, Hund's Rule is enforced by setting $J_0 = -23J_1^\perp$. As before, red points and blue points are even and odd under global orbital swap, $P_{d\bar{d}}$. We measured the expectation values for local orbital swap at the hole iron site, $P_{d\bar{d}}(\circ)$, and we found that the hole in even and odd parity states has

Table 1. Listed are groundstate expectation values of physical observables for one hole hopping over a $4 \times 4 \times 2$ lattice with the set of t - J model parameters used in Figs. 6-8: $t_2^\perp = 0$. Below, the QCP occurs at $J_{0c} = -1.733J_1^\perp$, and the integer coordinates (n_x, n_y) specify the momentum of the groundstate in units of $\pi/2a$.

Observable	$J_0 = 0$ @ $(0, 0)$	QCP @ $(0, 0)$	QCP @ $(2, 0)$	$J_0 = -23J_1^\perp$ @ $(1, 0)$
Fe triplets	7.90	11.50	13.48	14.96
$\mu_{\text{hFM}}^2/\mu_{\text{Fe}}^2$	0.93	0.60	0.26	0.06
$\mu_{\text{cSDW}}^2/\mu_{\text{Fe}}^2$	0.08	0.24	0.70	0.94
$P_{d\bar{d}}$	± 1	± 1	-1	-1
$P_{d\bar{d}}(\circ)$	∓ 0.06	± 0.02	-0.47	-0.94

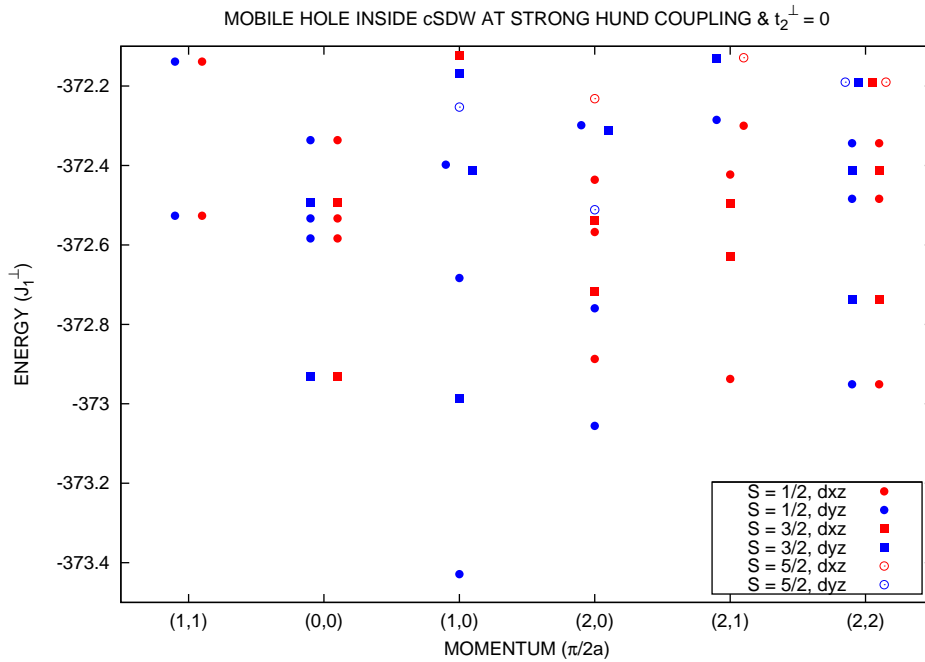


Figure 8. The low-energy spectrum of the two-orbital t - J model with one mobile hole hopping over a $4 \times 4 \times 2$ lattice is displayed at strong Hund's Rule coupling: $J_0 = -23J_1^\perp$. The remaining parameters are listed in the previous caption to Fig. 6.

orbital character that is respectively over 95 % $3d_{xz}$ and $3d_{yz}$. (See Table 1.) We have hence replaced the former labels with the latter ones in the legend to Fig. 8. The groundstate notably has spin-1/2, it carries momentum $(\pi/2a)\hat{x}(\hat{y})$, and it has orbital $3d_{yz}(3d_{xz})$ character. This is analogous to the groundstate momentum of $(\pi/2a)(\hat{x} \pm \hat{y})$ that is predicted for one mobile hole in a 2D Néel state by Kane, Lee and Read[28]. Table 1 lists ordered moments computed in the groundstate at momentum $(\pi/2a)\hat{x}(\hat{y})$. These moments combined with the low-energy spectrum indicate that the groundstate at thermodynamic hole densities x is a robust cSDW metal with Fermi surfaces that are centered at wavenumbers $(\pi/2a)\hat{x}$ and $(\pi/2a)\hat{y}$. This state is therefore unable to account for *any* of the Fermi surfaces that are observed experimentally in iron-pnictide

Table 2. Listed are the characteristic properties of observable versus hidden quantum-critical spin-wave excitations in the two-orbital Heisenberg model that corresponds to the two-orbital t - J model (1) in the absence of mobile holes. (See ref. [11], Fig. 5.)

spin wave	order parameter	2D momentum	Hund's Rule?	$P_{d\bar{d}}$ & $P'_{d\bar{d}}$
observable	$\mathbf{S}_{i,d+} + \mathbf{S}_{i,d-}$	$(\pi/a, 0)$ & $(0, \pi/a)$	obeyed	even
hidden	$\mathbf{S}_{i,d+} - \mathbf{S}_{i,d-}$	$(0, 0)$	violated	odd

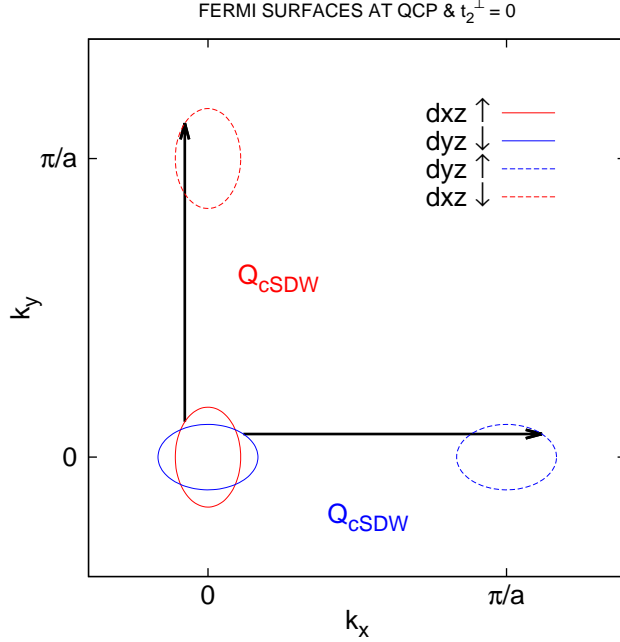


Figure 9. Conjectured nesting of Fermi surface pockets at QCP with nearest-neighbor inter-orbital hopping: $t_1^\perp \neq 0$ and $t_2^\perp = 0$. (Cf. figs. 2 and 7.)

systems.

The exact spectrum Fig. 7 at the QCP that separates a cSDW metal from a hidden half metal therefore indicates that coherent inter-orbital hole propagation exists near cSDW momenta in the case where inter-orbital hopping is purely across nearest neighbors. This contrasts with the prediction of dynamical suppression of inter-orbital hopping by the previous Schwinger-boson-slave-fermion mean-field theory at large s_0 . General agreement between the two calculations nevertheless exists. In particular, both the present exact results (Fig. 7) and the previous Schwinger-boson-slave-fermion mean-field theory analysis find a QCP at moderate Hund's Rule coupling, $-J_0$, where one-hole groundstates at zero 2D momentum and at cSDW momenta become degenerate. The mean-field theory indicates that the cSDW momentum of the degenerate groundstate in Fig. 7 is carried entirely by a spinwave that softens to zero excitation energy at the QCP. (See Figs. 3, 4 and 5.) Table 2 summarizes the nature of quantum-critical spinwave excitations for the corresponding Heisenberg model in the absence of mobile holes[11]. The key point to notice is that quantum-critical spinwaves at cSDW momenta

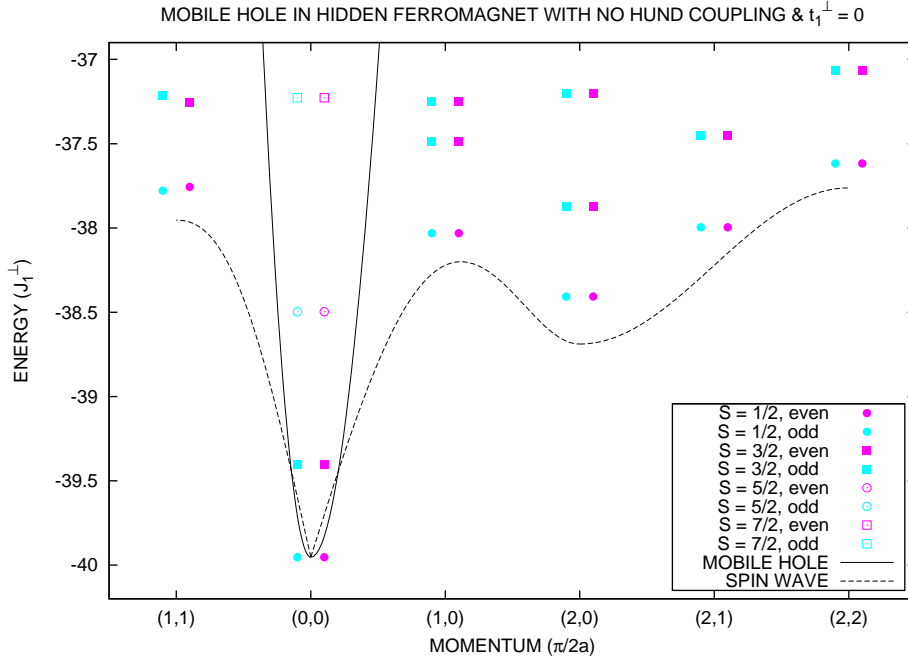


Figure 10. Shown is the low-energy spectrum of the two-orbital t - J model, Eq. (1), over a $4 \times 4 \times 2$ lattice with one hole, in the absence of Hund's Rule: $J_0 = 0$. The remaining parameters are $J_1^{\parallel} = 0$, $J_1^{\perp} > 0$, $J_2^{\parallel} = 0.3J_1^{\perp} = J_2^{\perp}$, $t_1^{\parallel} = -5J_1^{\perp}$, $t_1^{\perp} = 0$, $t_2^{\parallel} = 0$, $t_2^{\perp}(\hat{x} + \hat{y}) = -iJ_1^{\perp}$, and $t_2^{\perp}(-\hat{x} + \hat{y}) = +iJ_1^{\perp}$. A comparison with the hole spectrum, $\varepsilon_f(k) = \varepsilon_{\parallel}(\mathbf{k})$, and with the spin-wave spectrum, $\omega_b(k) = \omega_b^{(0)}(\mathbf{k})$, at large s_0 and $x = 0$ is also shown.

are *observable*, and they hence have even parity under $P_{d\bar{d}}$, while those at zero 2D momentum are *hidden*, and they hence have odd parity under $P_{d\bar{d}}$. [See Eqs. (51) and (52), and Fig. 3.] We have confirmed this by exact diagonalization of the corresponding Heisenberg model. The exact results displayed by Fig. 7 find one state at cSDW wavenumber $(\pi/a)\hat{x}(\hat{y})$ that is degenerate with groundstate at zero momentum. It is odd (even) under $P_{d\bar{d}}$. Combining the meanfield theory picture of the QCP with the present exact results then leads to the following conjecture: the critical cSDW spinwave at wavenumber $(\pi/a)\hat{x}$ relates the odd parity $3d_{yz}$ portion of the hole pockets centered at zero 2D momentum (Fig. 2) with its counterpart centered at the cSDW momentum, while the other critical cSDW spinwave at wavenumber $(\pi/a)\hat{y}$ relates the even parity $3d_{xz}$ portion of the hole pockets centered at zero 2D momentum with its counterpart centered at the other cSDW momentum. Further, we conjecture that the $3d_{xz}$ orbital is related to the $3d_{yz}$ orbital at the four hot spots in 2D momentum at which they coincide on the hole Fermi surface pockets by the hidden spin wave with odd parity under $P_{d\bar{d}}$ at zero 2D momentum. Figure 9 summarizes the conjectured reverse nesting mechanism.

Figures 10 and 11 show the exact spectrum of the two-orbital t - J model (1), respectively, in the absence of Hund's Rule coupling and at the QCP, but in the opposing case where inter-orbital hopping is purely across next-nearest neighbors. The model parameters, in particular, are $J_1^{\parallel} = 0$, $J_1^{\perp} > 0$, $J_2^{\parallel} = 0.3J_1^{\perp} = J_2^{\perp}$, $t_1^{\parallel} = -5J_1^{\perp}$, $t_1^{\perp} = 0$,

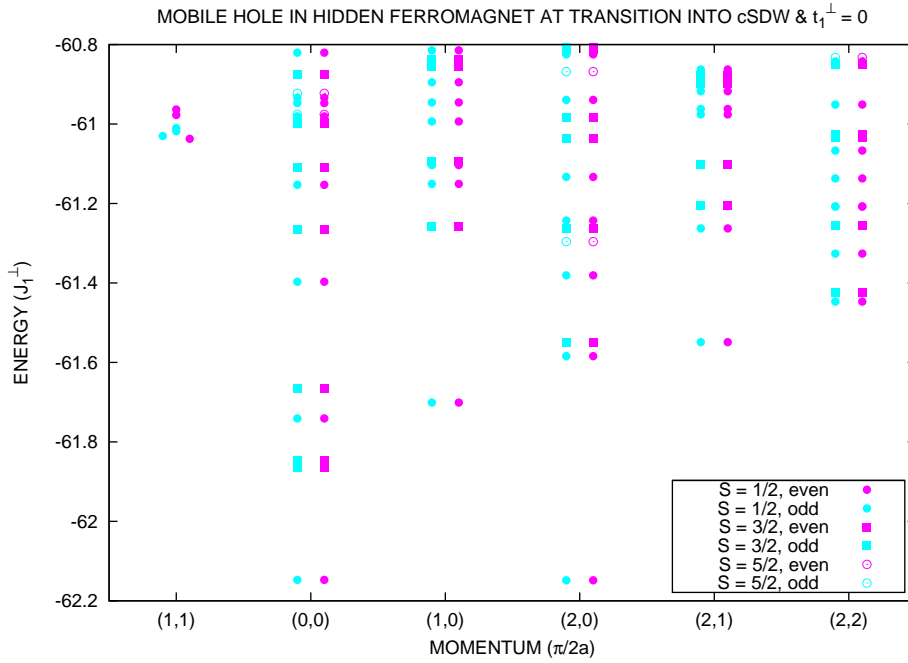


Figure 11. The low-energy spectrum of the two-orbital t - J model with one hole roaming over a $4 \times 4 \times 2$ lattice is displayed at the QCP that separates the cSDW from the hidden half-metal state: $J_{0c} = -2.26J_1^\perp$. The remaining set of parameters are listed in the previous caption to the Fig. 10.

$t_2^\parallel = 0$, $t_2^\perp(\hat{\mathbf{x}} + \hat{\mathbf{y}}) = -iJ_1^\perp$, and $t_2^\perp(-\hat{\mathbf{x}} + \hat{\mathbf{y}}) = +iJ_1^\perp$. Pink and light blue colors represent states that are respectively even and odd under the symmetry operation $P'_{d\bar{d}}$ that denotes swap of the $d\pm$ orbitals after the gauge transformation $e^{\pm i\pi/4}$. The critical Hund's Rule coupling at the QCP is $-J_{0c} = 2.26J_1^\perp$, which is very close to its value in the absence of inter-orbital hopping[18], $-J_{0c} = 2.27J_1^\perp$. Notice that both values are almost three times larger than the mean-field prediction at $x = 0$, $-J_{0c} = 0.8J_1^\perp$. The quantum-critical spectrum shown by Fig. 11 is also very close to the corresponding one in the absence of inter-orbital hopping up to a rigid energy shift that is relatively small[18]. Further, the moments for hidden ferromagnetic order and for cSDW order at the QCP that are listed in Table 3 match those obtained previously in the absence of inter-orbital hopping[18] to within 1%. We also computed the groundstate expectation values of modified orbital swap at the iron hole site, $P'_{d\bar{d}}(\circ)$, and these are listed in Table 3. A hole in a $3d_{x'z}$ orbital has even parity (+1) under it, while a hole in a $3d_{y'z}$ orbital has odd parity (-1) under it. Here, $x' = (x + y)/2^{1/2}$ and $y' = (y - x)/2^{1/2}$ are the 2D coordinates along the next-nearest neighbor links. Notice that $\langle P'_{d\bar{d}}(\circ) \rangle$ is generally small compared to unity, which means that the hole does *not* possess well-defined $3d_{x'z}$ or $3d_{y'z}$ orbital character at the QCP. To conclude, good agreement exists between exact results for the spectrum of the hidden half metal in the presence of purely next-nearest neighbor inter-orbital hopping and dynamical suppression of the latter as predicted by the previous Schwinger-boson-slave-fermion mean-field theory at large s_0 . It suggests

Table 3. Listed are groundstate expectation values of physical observables for one hole hopping over a $4 \times 4 \times 2$ lattice with the set of t - J model parameters used in Figs. 10 and 11: $t_1^\perp = 0$. Below, the QCP occurs at $J_{0c} = -2.26J_1^\perp$, and the integer coordinates (n_x, n_y) specify the momentum of the groundstate in units of $\pi/2a$.

Observable	$J_0 = 0$ @ $(0, 0)$	QCP @ $(0, 0)$	QCP @ $(2, 0)$
Fe triplets	7.84	12.09	13.20
$\mu_{\text{hFM}}^2/\mu_{\text{Fe}}^2$	0.94	0.53	0.32
$\mu_{\text{cSDW}}^2/\mu_{\text{Fe}}^2$	0.08	0.20	0.62
$P'_{d\bar{d}}$	± 1	± 1	± 1
$P'_{d\bar{d}}(\circ)$	∓ 0.07	∓ 0.06	± 0.13

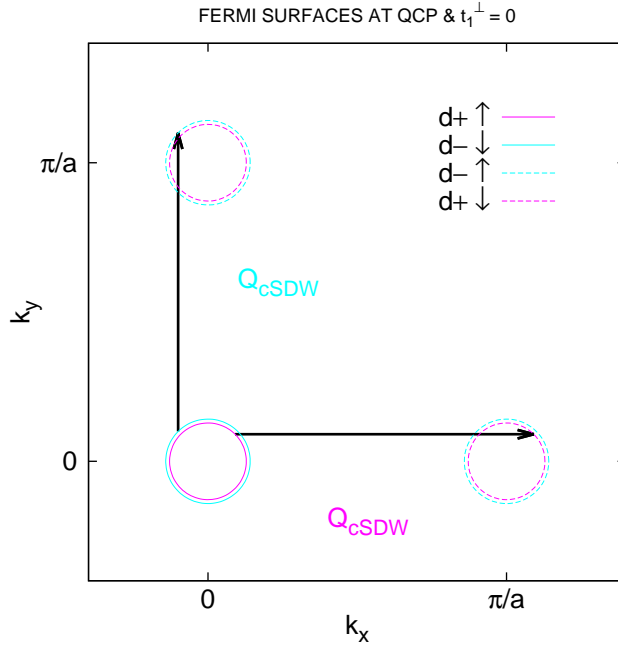


Figure 12. Predicted nesting of Fermi surface pockets at QCP with next nearest-neighbor inter-orbital hopping: $t_1^\perp = 0$ and $t_2^\perp \neq 0$. (Cf. figs. 2 and 11.)

the reverse Fermi surface nesting mechanism that is outlined by Fig. 12. Last, it is useful to point out that related behavior is predicted theoretically for a mobile hole in the Néel state over the square lattice, where nearest-neighbor hopping (t_1) is dynamically suppressed at low energy, leaving effective next nearest-neighbor hopping (t_2) within the same antiferromagnetic sublattice[31][36][37].

5. Discussion and Conclusions

Starting from a local-moment description of a cSDW over a square lattice of spin-1 iron atoms with mobile holes, we have succeeded in accounting for the nested Fermi surfaces pockets centered at zero 2D momentum and at cSDW momenta that are characteristic

of iron-pnictide high-temperature superconductors. In particular, zero-energy spin-wave excitations at cSDW momenta combine with hole Fermi surface pockets centered at zero 2D momentum to produce Fermi surface pockets centered at cSDW momenta. The former hole pockets exist because of proximity to a hidden half metal state with opposing polarized spin over $3d_{(x+iy)z}$ and $3d_{(x-iy)z}$ orbitals, respectively, which violates Hund's Rule. The isotropic ($d+$, $d-$) orbital basis that we choose notably maximizes the Hund's Rule coupling (see Appendix), and it leads to isotropic Heisenberg exchange coupling constants across neighboring spins on the square lattice of iron atoms. This orbital basis then very likely minimizes the net magnetic energy in the two-orbital t - J model (1) at fixed iron moment, $\langle |\sum_{\alpha} \mathbf{S}_{i,\alpha}|^2 \rangle^{1/2}$. Notice that the reverse Fermi-surface nesting effect uncovered here is a mirror image of weak-interaction descriptions for electronic structure in iron-pnictide high-temperature superconductors, where low-energy spin excitations centered at cSDW momenta are a *result* of Fermi surface nesting[2][38]. Unlike current descriptions of cSDW's in iron-pnictide materials that start from the weak-interaction limit[2][38], however, the present local-moment description predicts that hidden low-energy spin excitations across the $d+$ and $d-$ orbitals exist near zero 2D momentum because of proximity to the hidden half metal state.

It is useful to contrast our results with those of more ad hoc theoretical models that separate local moments from itinerant electrons[39][40]. Although such models are capable of simultaneously accounting for the spin-wave spectra and for the Fermi surfaces seen in iron-pnictide high-temperature superconductors and their parent compounds, they clearly have less predictive power by virtue of the explicit separation between the two phenomena. Early models for iron-pnictide systems that simply add Heisenberg exchange interactions and Hund coupling to one-electron hopping Hamiltonians that already include nested Fermi surfaces, but that do not project out double occupancy at an iron site-orbital, also suffer from this drawback in our opinion[41]. In particular, such models essentially operate in the weak-interaction limit, but they fail to link Fermi surface nesting to low-energy spin excitations at cSDW momenta in iron-pnictide high-temperature superconductors.

In summary, a mean-field theory analysis and an exact diagonalization study indicate that the two-orbital t - J model (1) for iron-pnictide high-temperature superconductors transits from a cSDW to a hidden half metal state with decreasing Hund's Rule coupling if off-diagonal magnetic frustration exists: e.g., $J_1^{d\pm, d\pm} = 0$, $J_1^{d\pm, d\mp} > 0$ and $J_2^{\alpha, \beta} > 0$. As shown by Fig. 1, intra-orbital hopping stabilizes antiferromagnetic order across the $d+$ and $d-$ orbitals, which characterizes the hidden half metal. This resembles the iron-pnictide phase diagram, where the cSDW is carrier poor while the superconductor is carrier rich. We therefore propose the hidden half metal state for the normal state of iron-pnictide high-temperature superconductors. This proposal is consistent with the low-energy spin-excitation spectrum and with the low-energy electronic structure shown by iron-pnictide high-temperature superconductors. Schwinger-boson-slave-fermion mean-field theory (51) predicts low-energy spinwaves that disperse anisotropically at cSDW momenta, $(\pi/a, 0)$ and $(0, \pi/a)$, near the quantum

critical point that separates the hidden half metal from the cSDW. The predicted dispersion of the spinwave spectrum, Fig. 3, notably shows a local maximum at the Néel wavenumber $(\pi/a, \pi/a)$, which agrees with inelastic neutron scattering studies of the parent compound CaFe_2As_2 [12]. Further, the anisotropic dispersion that we predict at the QCP for low-energy spinwaves at cSDW momenta is consistent with recent observations of the same in iron-pnictide superconductors[14][15][16][17].

Both the Schwinger-boson-slave-fermion mean-field theory formulation (53) and exact diagonalization of the two-orbital t - J model (1) predict Fermi surface pockets around zero 2D momentum and around cSDW momenta at the quantum critical point if the intra-orbital hopping is hole type (see Figs. 4d, 5 and 7). The Fermi surface pockets centered at $(0, 0)$ are due to the coherent motion of holes in the hidden half metal state (see Fig. 2). On the other hand, the low-energy electronic excitations about cSDW momenta are due to the combination of a hole excitation near the Fermi surfaces centered at zero 2D momentum with a low-energy spinwave that carries momentum near $(\pi/a, 0)$ or $(0, \pi/a)$. Figures 4b and 4c show that the electronic structure is a mixture of electron and hole types near those points in 2D momentum space. The dispersion velocity of the electron-type feature is notably given by the spin-wave velocity there! The above predictions are not inconsistent with the electronic structure shown by iron-pnictide high-temperature superconductors (cf. refs. [5] and [6]). The general features of the electronic structure that we predict near the quantum-critical point that separates the cSDW from the hidden half metal with the bare minimum of two $3d$ orbitals are also similar to what is predicted by band-structure calculations that include all five $3d$ orbitals. In particular, the checkerboard structure of the inequivalent iron atoms in iron-pnictide materials results in zone-folded Fermi surface pockets at $(\pi/a, \pi/a)$ that have only weak spectral weight[38].

Acknowledgments

Exact diagonalization of the two-orbital t - J model (1) was carried out on the SGI Altix 4700 at the AFRL DoD Supercomputer Resource Center. This work was supported in part by the US Air Force Office of Scientific Research under grant no. FA9550-09-1-0660 and by the FCT (Portugal) under grant PTDC/FIS/101126/2008.

Appendix

Here we calculate the Hund's Rule coupling in the 2D subspace spanned by the $3d_{xz}$ and $3d_{yz}$ orbitals in iron-pnictide materials. Consider the most general pair of basis states for such orbitals:

$$\phi(\mathbf{r}) = R_{3,2}(r)[(\cos \alpha_0)e^{-i\phi_0}Y_{2,+1}(\Omega) + (\sin \alpha_0)e^{+i\phi_0}Y_{2,-1}(\Omega)], \quad (0.1a)$$

$$\psi(\mathbf{r}) = R_{3,2}(r)[-(\sin \alpha_0)e^{-i\phi_0}Y_{2,+1}(\Omega) + (\cos \alpha_0)e^{+i\phi_0}Y_{2,-1}(\Omega)]. \quad (0.1b)$$

Notice that $\alpha_0 = 0$ or $\pi/2$ corresponds to the $3d_{(x+iy)z}/3d_{(x-iy)z}$ orbital basis, whereas $\alpha_0 = \pi/4$ and $\phi_0 = 0$ corresponds to the $3d_{xz}/3d_{yz}$ orbital basis. The exchange Coulomb integral is related to the Hund's Rule exchange coupling constant J_0 by

$$-\frac{1}{2}J_0 = \int d^3r_1 \int d^3r_2 \phi^*(\mathbf{r}_1)\psi(\mathbf{r}_1) \frac{e^2}{|\mathbf{r}_1 - \mathbf{r}_2|} \psi^*(\mathbf{r}_2)\phi(\mathbf{r}_2) \quad (0.2)$$

in general. In the present case, this yields

$$-\frac{1}{2}J_0 = \int d^3r_1 \int d^3r_2 R_{3,2}^2(r_1)[(\cos \alpha_0)^2 Y_{2,+1}^2(\Omega'_1) - (\sin \alpha_0)^2 Y_{2,-1}^2(\Omega'_1)] \\ \cdot \frac{e^2}{|\mathbf{r}_1 - \mathbf{r}_2|} R_{3,2}^2(r_2)[(\cos \alpha_0)^2 Y_{2,+1}^{*2}(\Omega'_2) - (\sin \alpha_0)^2 Y_{2,-1}^{*2}(\Omega'_2)],$$

where Ω' is the solid angle rotated by ϕ_0 about the z axis. The integrals over solid angles Ω'_1 and Ω'_2 can be performed in the standard way[42] by use of the mathematical identity

$$\frac{1}{|\mathbf{r}_1 - \mathbf{r}_2|} = \sum_{l=0}^{\infty} \frac{r_{<}^l}{r_{>}^{l+1}} \frac{4\pi}{2l+1} \sum_{m=-l}^l Y_{l,m}(\Omega'_1) Y_{l,m}^*(\Omega'_2) \quad (0.3)$$

combined with addition of angular momentum:

$$Y_{2,\pm 1}^2(\Omega) = \frac{1}{7} \left(\frac{15}{2\pi} \right)^{1/2} Y_{2,\pm 2}(\Omega) + \frac{1}{7} \left(\frac{10}{\pi} \right)^{1/2} Y_{4,\pm 2}(\Omega). \quad (0.4)$$

Performing the remaining radial integrals after substitution of the hydrogenic radial wave function

$$R_{3,2}(r) = \frac{2}{81} \left(\frac{2}{15a_0^3} \right)^{1/2} \left(\frac{r}{a_0} \right)^2 e^{-r/3a_0} \quad (0.5)$$

then yields the final result

$$-\frac{1}{2}J_0 = \frac{1}{(2 \cdot 3)^5 (5 \cdot 7)^2} \left[3 I_2 + 5 \left(\frac{2}{3} \right)^2 I_4 \right] \frac{e^2}{a_0} (\cos^4 \alpha_0 + \sin^4 \alpha_0), \quad (0.6)$$

where

$$I_4 = \frac{12!}{2^{12}} \left(\frac{2}{11} - \frac{1}{12} \right) \quad (0.7)$$

and

$$I_2 = \frac{12!}{2^{12}} \left(\frac{2^3}{9} - 3 \frac{2^2}{10} + 3 \frac{2}{11} - \frac{1}{12} \right) \quad (0.8)$$

are the strengths of the integrals due to the $l = 4$ and $l = 2$ channels, respectively. Note that the binomial-like series that appear above result from the difference

$$(5 - l)! - 2^{-(6-l)} s_{11}^{(5-l)}(1/2),$$

where $s_n^{(m)}(x)$ is the m^{th} derivative of the finite geometric series sum $s_n(x) = \sum_{k=0}^n x^k$. The Hund's Rule coupling is then

$$-J_0 = \frac{1}{30.3082} \frac{e^2}{2a_0} (\cos^4 \alpha_0 + \sin^4 \alpha_0). \quad (0.9)$$

Notice that $\cos^4 \alpha_0 + \sin^4 \alpha_0 = 1 - \frac{1}{2} \sin^2 2\alpha_0$, which reaches its maximum value of unity at $\alpha_0 = 0$ or $\pi/2$ and its minimum value of $1/2$ at $\alpha_0 = \pi/4$. We conclude that the Hund's Rule coupling is largest in the isotropic $3d_{(x+iy)z}/3d_{(x-iy)z}$ orbital basis, while it is smallest in the anisotropic $3d_{xz}/3d_{yz}$ orbital basis from Chemistry.

It is useful to compare the maximum Hund's Rule coupling in the isotropic $3d_{(x+iy)z}/3d_{(x-iy)z}$ orbital basis with the on-site Coulomb repulsion in that case:

$$U_0 = \int d^3 r_1 \int d^3 r_2 R_{3,2}^2(r_1) |Y_{2,1}(\Omega_1)|^2 \frac{e^2}{|\mathbf{r}_1 - \mathbf{r}_2|} R_{3,2}^2(r_2) |Y_{2,1}(\Omega_2)|^2. \quad (0.10)$$

Addition of angular momentum yields the identity

$$|Y_{2,1}(\Omega)|^2 = \frac{1}{7\pi} P_0(\cos \theta) + \frac{5}{28\pi} P_2(\cos \theta) - \frac{3}{7\pi} P_4(\cos \theta) \quad (0.11)$$

in terms of Legendre polynomials. Substituting it above, with $P_l(\cos \theta) = [4\pi/(2l+1)]^{1/2} Y_{l,0}(\Omega)$, along with the mathematical identity (0.3), yields the result

$$U_0 = \frac{1}{2^6 3^5 5^2} \left[I_0 + \frac{1}{7^2} I_2 + \left(\frac{4}{3 \cdot 7} \right)^2 I_4 \right] \frac{e^2}{a_0} \quad (0.12)$$

for the Coulomb integral, where

$$I_0 = \frac{12!}{2^{12}} \left(\frac{2^5}{7} - 5 \frac{2^4}{8} + 10 \frac{2^3}{9} - 10 \frac{2^2}{10} + 5 \frac{2}{11} - \frac{1}{12} \right) \quad (0.13)$$

is the strength of the integral in the $l = 0$ channel. The ratio of the on-site Coulomb repulsion (0.12) to the Hund's Rule coupling (0.6) is then

$$-\frac{2U_0}{J_0} = 10.6743. \quad (0.14)$$

Study of the exchange integral (0.2) yields that this ratio coincides with the ratio $J_1^{d+,d+}(\text{drct})/J_1^{d+,d-}(\text{drct})$ in the regime $a_0 \gg a$.

References

- [1] Y. Kamihara, T. Watanabe, M. Hirano, and H. Hosono, J. Am. Chem. Soc. 130, 3296 (2008).
- [2] J. Dong, H. J. Zhang, G. Xu, Z. Li, G. Li, W. Z. Hu, D. Wu, G. F. Chen, X. Dai, J. L. Luo, Z. Fang, N. L. Wang, Euro. Phys. Lett. **83**, 27006 (2008).
- [3] V.B. Zabolotnyy, D.S. Inosov, D.V. Evtushinsky, A. Koitzsch, A.A. Kordyuk, G.L. Sun, J.T. Park, D. Haug, V. Hinkov, A.V. Boris, C.T. Lin, M. Knupfer, A.N. Yaresko, B. Buchner, A. Varykhalov, R. Follath and S.V. Borisenko, Nature **457**, 569 (2009).

- [4] J. Fink, S. Thirupathaiah, R. Ovsyannikov, H. A. Durr, R. Follath, Y. Huang, S. deJong, M. S. Golden, Yu-Zhong Zhang, H. O. Jeschke, R. Valenti, C. Felser, S. Dastjani Farahani, M. Rotter, and D. Johrendt, *Phys. Rev. B* **79**, 155118 (2009).
- [5] V. Brouet, M. Marsi, B. Mansart, A. Nicolaou, A. Taleb-Ibrahimi, P. Le Fevre, F. Bertran, F. Rullier-Albenque, A. Forget, and D. Colson, *Phys. Rev. B* **80**, 165115 (2009).
- [6] V. Brouet, M. Fuglsang Jensen, A. Nicolaou, A. Taleb-Ibrahimi, P. Le Fevre, F. Bertran, A. Forget, and D. Colson, arXiv:1105.5604 .
- [7] C. de la Cruz, Q. Huang, J.W. Lynn, J. Li, W. Ratcliff, J.L. Zarestky, H.A. Mook, G.F. Chen, J.L. Luo, N.L. Wang and P. Dai, *Nature* **453**, 899 (2008).
- [8] Q. Si and E. Abrahams, *Phys. Rev. Lett.* **101**, 076401 (2008).
- [9] J.P. Rodriguez and E.H. Rezayi, *Phys. Rev. Lett.* **103**, 097204 (2009).
- [10] B. Schmidt, M. Siahatgar, P. Thalmeier, *Phys. Rev. B* **81**, 165101 (2010).
- [11] J.P. Rodriguez, *Phys. Rev. B* **82**, 014505 (2010).
- [12] Jun Zhao, D. T. Adroja, Dao-Xin Yao, R. Bewley, Shiliang Li, X. F. Wang, G. Wu, X. H. Chen, Jiangping Hu, Pengcheng Dai, *Nature Physics* **5**, 555 (2009).
- [13] S.O. Diallo, V.P. Antropov, T.G. Perring, C. Broholm, J.J. Pulikkotil, N. Ni, S.L. Bud'ko, P.C. Canfield, A. Kreyssig, A.I. Goldman and R.J. McQueeney, *Phys. Rev. Lett.* **102**, 187206 (2009).
- [14] C. Lester, Jiun-Haw Chu, J. G. Analytis, T. G. Perring, I. R. Fisher, S.M. Hayden, *Phys. Rev. B* **81**, 064505 (2010).
- [15] J. T. Park, D. S. Inosov, A. Yaresko, S. Graser, D. L. Sun, Ph. Bourges, Y. Sidis, Yuan Li, J.-H. Kim, D. Haug, A. Ivanov, K. Hradil, A. Schneidewind, P. Link, E. Faulhaber, I. Glavatsky, C. T. Lin, B. Keimer, V. Hinkov, *Phys. Rev. B* **82**, 134503 (2010).
- [16] H.-F. Li, C. Broholm, D. Vaknin, R. M. Fernandes, D. L. Abernathy, M. B. Stone, D. K. Pratt, W. Tian, Y. Qiu, N. Ni, S. O. Diallo, J. L. Zarestky, S. L. Bud'ko, P. C. Canfield, R. J. McQueeney, *Phys. Rev. B* **82**, 140503(R) (2010).
- [17] M Liu, L. W. Harringer, H. Luo, M. Wang, R.A. Ewings, T. Guidi, H. Park, K. Haule, G. Kotliar, S.M. Hayden and P. Dai, *Nature Physics* (2012).
- [18] J.P. Rodriguez, M.A.N. Araujo, P.D. Sacramento, *Phys. Rev. B* **84**, 224504 (2011).
- [19] J.M. Foster and S.F. Boys, *Rev. Mod. Phys.* **32**, 300 (1960).
- [20] C. Edmiston and K. Ruedenberg, *Rev. Mod. Phys.* **35**, 457 (1963).
- [21] P. Fulde, *Electron Correlations in Molecules and Solids* (Springer-Verlag, Berlin, 1993).
- [22] S. Raghu, Xiao-Liang Qi, Chao-Xing Liu, D. Scalapino, Shou-Cheng Zhang, *Phys. Rev. B* **77**, 220503(R) (2008).
- [23] P.W. Anderson, *Phys. Rev.* **79**, 350 (1950).
- [24] F. Ma, Z.-Y. Lu and T. Xiang, *Phys. Rev. B* **78**, 224517 (2008).
- [25] Z.-Y. Lu, F. Ma and T. Xiang, *J. Phys. Chem. Solids* **72**, 319 (2011).
- [26] B. Shraiman and E. Siggia, *Phys. Rev. Lett.* **60**, 740 (1988).
- [27] S. Trugman, *Phys. Rev. B* **37**, 1597 (1988).
- [28] C.L. Kane, P.A. Lee and N. Read, *Phys. Rev. B* **39**, 6880 (1989).
- [29] A. Auerbach and B. E. Larson, *Phys. Rev. B* **43**, 7800 (1991).
- [30] D.P. Arovas and A. Auerbach, *Phys. Rev. B* **38**, 316 (1988).
- [31] A. Auerbach, *Interacting Electrons and Quantum Magnetism* (Springer-Verlag, New York, 1998).
- [32] A. Auerbach and D.P. Arovas, *Phys. Rev. Lett.* **61**, 617 (1988).
- [33] Y. Ran, F. Wang, H. Zhai, A. Vishwanath, and D.-H. Lee, *Phys. Rev. B* **79**, 014505 (2009).
- [34] C. Lanczos, *J. Research National Bureau of Standards* **45** (4), 255 (1950).
- [35] R.B. Lehoucq, D.C. Sorensen and C. Yang, *ARPACK Users' Guide* (SIAM, Philadelphia, 1998).
- [36] A. Auerbach, *Phys. Rev. B* **48**, 3287 (1993).
- [37] C.L. Kane, P.A. Lee, T.K. Ng, B. Chakraborty and N. Read, *Phys. Rev. B* **41**, 2653 (1990).
- [38] S. Graser, T.A. Maier, P.J. Hirschfeld and D.J. Scalapino, *New J. Phys.* **11**, 025016 (2009).
- [39] S.-P. Kou, T. Li, Z.-Y. Weng, *Euro. Phys. Lett.* **88**, 17010 (2009).
- [40] W. Lv., F. Kruger and P. Phillips, *Phys. Rev. B*, **82**, 045125 (2010).

- [41] K. Seo, B.A. Bernevig and J. Hu, Phys. Rev. Lett. **101**, 206404 (2008).
- [42] H.A. Bethe and R. Jackiw, *Intermediate Quantum Mechanics* (Westview Press, 1997).